



Norwegian University of
Science and Technology

Riser lift system for deep sea mining

Haiying Mao

Marine Technology

Submission date: June 2018

Supervisor: Svein Sævik, IMT

Norwegian University of Science and Technology
Department of Marine Technology



Norwegian University of
Science and Technology

Riser lift system for deep sea mining

Haiying Mao

MASTER THESIS

Department of Marine Technology

Norwegian University of Science and Technology

June 2018

Trondheim, Norway

Supervisor : Svein Sævik

Preface

I am a master studying in the Nordic Master Programme in Maritime Engineering. I spent my first academic year in the Aalto University. I got a lot of knowledge and help from there. This master thesis has been finished at the Norwegian University of Science and Technology. It is a great summary of my learning results in the second academic year.

This master thesis focuses on the riser lift system applied in the deep sea mining. I have learned a lot of knowledge about riser, mining and structure analysis. I would like to thank my supervisor Prof. Svein Sævik at the Department of Marine Technology, NTNU. He gave me a great help on guidance and feedback. And I also need to thank Dr. Yuna Zhao from NTNU, she helped me a lot on the SIMA modelling. Finally, I want to thank my parents for everything.

Trondheim, June 2018

Haiying Mao

Haiying Mao

Summary

The growing global demand for rare metals and the declining land mineral resources impel the research on exploring seabed minerals resources. Based on this requirement, some research projects about deep sea mining are ongoing. Among them, this thesis focuses on one case, which is within the Norwegian interest zone along the North-East part of the Mid-Atlantic Ridge outside Svalbard, the water depth is in excess of 3000 m.

For deep sea mining in the North Atlantic at a water depth of over 3,000 meters, there are significant challenges with regard to operating the riser lift system needed to transport the minerals from the seabed to the sea surface. The objective of this master thesis is to explore the limitations of operating such a riser system at large water depths with focus on the dynamic behaviour of the system. In addition, based on the dynamic response and the limiting criteria, perform the fatigue analysis to find the fatigue life of the riser lift system. Then, comparing the difference of the dynamic behavior and fatigue life of the riser lift system under the two topside connection conditions.

The riser lift system may be in the form of a subsea pump and a vertical riser transporting slurry flow (water and rock). A case study was performed for representative sea states with regard to two working conditions by the Riflex module of SIMA. The top of the riser was connected to a vessel, and the end of the riser was connected to a pump. The length of the riser was 2970m, and the water depth was 3000m. Two working conditions were studied: The operating condition where the top of the riser was connected to the vessel by a pin joint. For the installation condition, the top of the riser was completely fixed to the vessel. The external load of the riser lift system is just considered the Morison load, which contains the current load, the wave load and the resulting vessel motion. The scatter diagram of the northern North Sea was applied as basis for this case.

The results of this study indicated that the topside connection of the riser has a big impact on the riser. The bending moment and stress of the riser with fixed topside connection is much larger than it with pinned topside connection. Moreover, all the dynamic response of riser is increasing as the growing of the wave significant height. The limiting sea states of the riser with pinned topside connection is when the wave significant height is larger than 7m. And to the fixed topside connection is when the wave significant height is larger than 2m. In addition, in this case, the fatigue life of the riser is too short whatever the topside connection is. In general, it is difficult to apply a steel riser under these conditions, even if the vortex induced vibration is not considered in this study.

Contents

Preface.....	III
Summary.....	V
Contents.....	VII
List of Figures.....	IX
List of Tables.....	XI
Nomenclature.....	XII
1. Introduction.....	1
1.1. Motivation.....	1
1.2. Objective.....	1
1.3. Scope and limitation.....	1
1.4. Chapter overview.....	2
2. Literature review.....	3
2.1. Vertical steel riser behavior.....	3
2.2. Ocean mining.....	5
2.2.1. Mining minerals.....	5
2.2.2. Mining system.....	6
2.2.3. Mining support vessel.....	7
3. DNV GL rules and regulations.....	8
3.1. DNV-OS-F201: Dynamic risers.....	8
3.1.1. Loads.....	8
3.1.2. Design criteria for riser pipes.....	9
3.1.3. Combined loading criteria of ULS.....	10
3.2. DNV-OS-F204: Riser fatigue.....	11
3.3. DNV-OS-C203: Fatigue design of offshore steel structures.....	12
4. Non-linear time domain analysis.....	13
4.1. Finite elements formulations.....	13
4.2. Load models.....	14
4.2.1. Hydrodynamic loads.....	14
4.2.2. Wave kinematics.....	15
4.2.3. Vessel motion.....	17
4.3. Analysis procedure.....	17
4.3.1. Static analysis.....	17
4.3.2. Dynamic analysis.....	18
4.3.3. Fatigue analysis.....	20
5. Modelling by SIMA.....	22
5.1. The environment condition.....	23
5.2. Riser system.....	25
5.2.1. Boundary condition.....	26
5.2.2. Riser line types.....	26
5.2.3. Components.....	27
5.2.4. Cross section.....	28

5.3. Support vessels.....	30
5.4. Static and dynamic calculation parameter.....	32
5.4.1. The static calculation parameter.....	32
5.4.2. The dynamic calculation parameter.....	33
5.5. Input data.....	34
6. Pinned topside connection analysis results.....	35
6.1. Quasi-static analysis.....	35
6.1.1. Effective tension.....	35
6.2. Eigenfrequency.....	36
6.3. Dynamic analysis.....	37
6.3.1. Vertical Displacement.....	37
6.3.2. Axial tension.....	39
6.3.3. Bending moment.....	41
6.3.4. Riser stress.....	44
6.4. Fatigue analysis.....	46
7. Fixed topside connection analysis results.....	49
7.1. Quasi-static analysis.....	49
7.1.1. Effective tension.....	49
7.2. Dynamic analysis.....	50
7.2.1. Vertical Displacement.....	50
7.2.2. Axial tension.....	51
7.2.3. Bending moment.....	53
7.2.4. Riser stress.....	54
7.3. Fatigue analysis.....	56
8. Comparison and analysis.....	58
8.1. Quasi-static analysis.....	58
8.2. Dynamic analysis.....	58
8.2.1. Vertical displacement.....	58
8.2.2. Axial force.....	59
8.2.3. Bending moment.....	59
8.2.4. Riser stress.....	61
8.3. Limiting sea states.....	62
8.4. Fatigue analysis.....	64
9. Conclusion and further work.....	65
9.1. Conclusion.....	65
9.2. Further work.....	65
Reference.....	66

List of Figures

Figure 2-1 . Schematic of SMS mining technology and plan for the Solwara 1 deposit off Papua New Guinea[7].....	6
Figure 2-2 . The model for the world’s first seabed mining vessel[8].....	7
Figure 4-1 . Nodal degrees of freedom for beam element[15].....	13
Figure 4-2 . The fatigue analysis procedure.....	20
Figure 5-1 . The riser model from SIMA.....	22
Figure 5-2 .The relationship between the current velocity and the water depth.....	23
Figure 5-3 . Scatter diagram of the northern North Sea[21].....	24
Figure 5-4 . The wave spectrum of the significant on Hs is 4m and Tp is 8s.....	25
Figure 5-5 . Riser system definition terms.....	25
Figure 5-6 . Riser line types.....	27
Figure 5-7 . The local coordinate system(x,y,z) of riser.....	28
Figure 5-8 . The cross section properties of the riser.....	29
Figure 5-9 . The hydrodynamic force coefficient for riser.....	30
Figure 5-10 . The local coordinate system of the semi-submersible platform.....	31
Figure 5-11 . The RAOs of vessel translating motion.....	31
Figure 5-12 . The RAOs of vessel rotating motion.....	32
Figure 5-13 . The specific static calculation parameter settings.....	32
Figure 5-14 . The specific dynamic calculation parameter settings.....	33
Figure 6-1 . The quasi-static effective tension of the riser.....	36
Figure 6-2 . Tension power spectrum on Hs=1m, Tp=5s.....	37
Figure 6-3 . The displacement standard deviation of the riser on Hs=2m, Tp=8s.....	38
Figure 6-4 . The displacement of the final node of the riser on Hs=2m, Tp=8s.....	38
Figure 6-5 . The force envelope curve of the riser on Hs=2m, Tp=8s.....	39
Figure 6-6 . The axial tension of element 1 of the riser on Hs=2m, Tp=8s.....	40
Figure 6-7 . The total bending moment along the riser on Hs=2m, Tp=8s.....	41
Figure 6-8 . The partial enlarged view of total bending moment along the riser on Hs=2m, Tp=8s.....	41
Figure 6-9 . The y-direction bending moment along the riser on Hs=2m, Tp=8s.....	42
Figure 6-10 . The z-direction bending moment along the riser on Hs=2m, Tp=8s.....	42
Figure 6-11 . The schematic diagram of eight equal diversion points along the outer wall of the riser.....	44
Figure 6-12 . The resultant stress in the time domain of the point 3 on Hs=1m, Tp=5s.....	45
Figure 6-13 . The fatigue life of riser with pinned topside connection by resultant stress.....	47
Figure 6-14 . The fatigue life of riser with pinned topside connection by only axial tension stress.....	47
Figure 7-1 . The quasi-static effective tension of the riser.....	49
Figure 7-2 . The displacement standard deviation of the riser on Hs=2m, Tp=8s.....	50
Figure 7-3 . The displacement of the final node of the riser on Hs=2m, Tp=8s.....	50
Figure 7-4 . The force envelope curve of the riser on Hs=2m, Tp=8s.....	51

Figure 7-5 . The axial tension of element 1 of the riser on $H_s=2m$, $T_p=8s$	52
Figure 7-6 . The total bending moment along the riser on $H_s=2m$, $T_p=8s$	53
Figure 7-7 . The partial enlarged view of total bending moment along the riser on $H_s=2m$, $T_p=8s$	53
Figure 7-8 . The resultant stress in the time domain of the point 3 on $H_s=1m$, $T_p=5s$	55
Figure 7-9 . The fatigue life of riser with fixed topside connection by resultant stress.....	56
Figure 7-10 . The fatigue life of riser with fixed topside connection by only axial tension stress.....	57
Figure 7-11 . The fatigue life of riser with fixed topside connection by only bending moment stress.....	57
Figure 8-1 . The vertical displacement of end of the riser with pinned topside connection...	58
Figure 8-2 . The axial tension of top of the riser with pinned topside connection.....	59
Figure 8-3 . The maximum bending moment of riser with pinned topside connection.....	60
Figure 8-4 . The maximum bending moment of riser with fixed topside connection.....	60
Figure 8-5 . The maximum stress of riser with pinned topside connection.....	61
Figure 8-6 . The maximum stress of riser with fixed topside connection.....	61

List of Tables

Table 2-1 . The parameter of the example ship[8].....	7
Table 3-1 . The safety class resistance factor.....	11
Table 3-2 . The material resistance factor.....	11
Table 3-3 . Design fatigue factors DFF.....	12
Table 5-1 . The various sea states for riser operating.....	24
Table 5-2 . The total data used in this study.....	34
Table 6-1 . The absolute value of maximum vertical displacement (m) of the end node of selected sea states.....	39
Table 6-2 . The maximum axial tension(MN) of the element 1 of selected sea states.....	40
Table 6-3 . The location of the total maximum bending moment along the riser of selected sea states.....	43
Table 6-4 . The total maximum bending moment(Nm) of the riser of selected sea states.....	43
Table 6-5 . The maximum stress (Mpa) of selected sea states.....	45
Table 6-6 . The probability of the occurrence of selected sea states.....	46
Table 7-1 . The absolute value of maximum vertical displacement (m) of the end node of selected sea states.....	51
Table 7-2 . The maximum axial tension(MN) of the element 1 of selected sea states.....	52
Table 7-3 . The total maximum bending moment (KNm) of riser of selected sea states.....	54
Table 7-4 . The maximum stress (Mpa) of the riser of selected sea states.....	55
Table 8-1 . The limiting sea states for operating the riser system.....	62
Table 8-2 . Riser stress checking by DNV rules in the pinned topside connection.....	63
Table 8-3 . Riser stress checking by DNV rules in the fixed topside connection.....	63
Table 8-4 . The riser fatigue life in different conditions.....	64

Nomenclature

Abbreviations

VIV	Vortex Induced Vibration
SMS	Seafloor Massive Sulfides
DNV	Det Norsk Veritas
FLS	Fatigue Limit State
ULS	Ultimate Limit State
RAOs	Response Amplitude Operators

Symbols

M_d	Design bending moment
T_d	Design effective tension
M_k	The (plastic) bending moment resistance
T_k	The plastic axial force resistance
f_y	Yield strength to be used in design
α_c	Flow stress parameter accounting for strain hardening
γ_{sc}	Safety class resistance factor
γ_m	Material resistance factor
N	Predicted number of cycles to failure of stress range $\Delta\sigma$
$\Delta\sigma$	Stress range
$\log \bar{a}$	Intercept of log N -axis by S-N curve
m	Negative inverse slope of S-N curve
ΔR	Element force vector
K_m	Material stiffness matrix
K_σ	Initial stiffness matrix
Δr	Element nodal displacement vector
F_w	Fluid force
a_c	Fluid acceleration relative to earth
C_A	Added mass coefficient for the body
a_r	Fluid acceleration relative to the body

V_r	Current velocity relative to the body
C_D	Drag coefficient
ω_p	Peak frequency
T_p	Peak periods
H_s	Significant height
\mathbf{R}^I	Inertia force vector
\mathbf{R}^D	Damping force vector
\mathbf{R}^S	Internal structural reaction force vector
\mathbf{R}^E	External force vector
D_L	Long-term fatigue damage
N_S	Number of discrete sea states in the wave scatter diagram
P_i	Sea state probability
D_i	Short term fatigue damage
k	Structure stiffness
ω_n	Eigenfrequency
D_o	Riser overall diameter
D_i	Riser internal diameter
D_b	Diameter of the whole riser (contains the buoyancy layer)
ρ_r	Density of riser material (steel)
ρ_m	Mineral density
ρ_b	Buoyancy layer density
ρ_w	Density of the sea water
t	Riser thickness

1. Introduction

1.1. Motivation

With the growing global demand for strategic rare metals, the prices are rising. Even if the deep sea mining is still controversial due to the environment problem, there are ongoing efforts would wish to explore sea bed minerals as the land resources are gradually declining. As such, deep sea mining is an emerging industry and several research projects are ongoing. Within the Norwegian interest zone along the North-East part of the Mid-Atlantic Ridge outside Svalbard, the water depth is in excess of 3000 m. Around this area, ocean water penetrates several kilometres down towards the centre of the Earth where the crust is fractured. Liquid magma heats the water to about 400 degree centigrade before the water squirts back out again as an underwater geyser. The ocean water draws minerals and metals out of the Earth's crust and carries these back up to the seabed. Gold, silver, copper, cobalt, zinc, and lead are all deposited when the hot springs meet the cold ocean water[1]. Therefore, researchers are investigating the feasibility of deep sea mining in this area.

1.2. Objective

For deep sea mining in the North Atlantic at a water depth of over 3,000 meters, there are significant challenges with regard to operating the riser lift system needed to transport the minerals from the seabed to the sea surface. The riser lift system may be in the form of a subsea pump and a vertical riser transporting slurry flow (water and rock). A case study was performed for representative sea states with regard to two working conditions by the Riflex module of SIMA. The aim of this master thesis is to explore the limitations of operating such a riser system at large water depths with focus on the dynamic behaviour of the system. In addition, based on the dynamic response and the limiting criteria, perform the fatigue analysis to find the fatigue life of the riser lift system. Then, comparing the difference of the dynamic behavior and fatigue life of the riser lift system under the two topside connection conditions.

1.3. Scope and limitation

The scope of the thesis is narrowed by only applying one scatter diagram of the northern North Sea as the representative sea states for operating the riser system. Moreover, the riser lift system model was simplified by ignoring the booster stations along the riser and the flexible jumper which connects the pump to the seabed. The external load of the riser lift system is just considered the Morison load, which

contains the current load, the wave load and the resulting vessel motion. However the vortex induced vibration is not included in this thesis.

1.4. Chapter overview

Chapter 2: *Literature review* covers the literature study, providing the existed research results and related knowledge of ocean mining. Chapter 3: *DNV GL rules and regulations* gives the related DNV rules and standards which needed to be referred to in this thesis. Chapter 4: *Non-linear time domain analysis* presents a concise theoretical introduction for the non-linear time domain analysis method. Chapter 5: *Modelling by SIMA* describes the detailed modelling procedure of riser system and lists the total used parameters. Chapter 6 and Chapter 7 lists the results of pinned topside connection analysis and fixed topside connection analysis, respectively. The comparison of the two topside connection analysis and the limiting sea states for operating the riser system are shown in Chapter 8. Finally, the conclusion and suggestion for the further work are discussed in Chapter 9.

2. Literature review

2.1. Vertical steel riser behavior

Recently, the application of the riser in the drilling and mining field has gradually shifted from the shallow sea to the deep sea. At the same time, related research and analysis have also undergone changes. However, because these studies were conducted in recent years, few articles and data are available for reference and comparison. Fortunately, there are some research papers about the dynamic and fatigue analysis of the riser. Even if most of the research is about theoretical methods and takes the example of the risers applied in the shallow water and ordinary sea states. The focus of the dynamic and fatigue analysis of the riser and related considerations are very worthy of reference.

Burke (1974)[2] presents one mathematical model which can be used into the analysis of the riser, and tries to show the consequence of applying the riser into deeper water. The analysis model used in Burke (1974) is based on the linear differential equation applied to the beam column under the lateral loads in the vertical plane. Moreover, the linear differential equation can be solved by the numerical integration method, by specifying the force distribution along the length and implementing the boundary conditions at each end. In the paper, the top of the riser is connected to the vessel, static analysis is performed under the horizontal displacement at the top of the riser caused by the vessel motion and the lateral load caused by the ocean currents. And the dynamic analysis is performed under the vessel motions and sinusoidal wave forces. During this case, the riser is analyzed for water depths of 120m to 600m.

The static results of Burke (1974) shows that the tension stresses of the unbuoyed riser increases significantly as the water depth increases. As a consequent, additional buoyancy is considered added to the longer marine risers to reduce the submerged riser weight. According to this, the tension requirements to support the riser can be decreased. However, the top bending stress of the buoyed riser is much greater than that of the unbuoyed riser. This is due to the top tension of the buoyed riser is lower, and the riser diameter used to compute the drag force is increased while adding buoyant material. Therefore, considering both of the tension stress and bending stress, how to apply the buoyant is very important. And it will also be focused on in this thesis.

The dynamic results of Burke (1974) shows that the response of the riser to larger waves results in greater speed and higher damping, which in turn reduces the resonant response of the riser. Therefore, it is found that when the riser responds to waves, especially when the period of the wave is close to the natural vibration period

of the riser, the response result is a strong nonlinear function of the wave height. Moreover, compared to the wave forces acting directly on the riser, the vessel motion caused by the waves is a more significant factor for the dynamic response of the riser. Therefore, the motion characteristics of vessels which are connected to risers are also a main factor in the design of the riser and defining the limitation in terms of the sea states.

In conclusion, the static and the dynamic response of the riser are both significant factors to be considered when the water depth is increasing. In addition to the motion characteristics of the vessel.

There is no discussion on the fatigue analysis of the riser in this paper. Fortunately, it can be found in Chen et al. (2012)[3].

The two ends of riser model in Chen et al. (2012) were constrained. In details, the top end of the riser was pinned to the drilling vessel and the bottom end of the riser was below the seabed. The water depth in this case was around 100m, corresponding to a shallow water environment condition. The fatigue model in this paper was based on application of the Rain-flow counting method, S-N curve and Miner-Palmgren rule. The results show the fatigue damage of the bottom of the riser decreased when the soil stiffness of seabed was increased; increasing the thickness of the riser can inhibit fatigue damage effectively; where as increasing the weld eccentricity of riser can significantly increase fatigue damage. Although the influencing factors of the fatigue damage in this paper are different from the thesis, the method of fatigue analysis include similarities.

Mukundan et al. (2009)[4] shows that fatigue damage will also be affected by the vortex induced vibration. The reason is that the long flexible cylinders (e.g. risers) exposed to the marine environment encounter ocean currents leading to vortex induced vibration (VIV). These oscillations, often driven at high frequencies over extended periods of time may result in structural failure of the member due to fatigue damage accumulation.

However, in this study, the main point is to find the effect by the different wave conditions on the riser dynamic response, rather than the vortex induced vibration caused by the ocean current. Therefore, the Morison's load, which contains the current load, the wave load and the resulting vessel motion, is applied on the riser lift system. The vortex induced vibration will not be considered in the following analysis procedure.

2.2. Ocean mining

Most of existing vertical steel riser cases are related to offshore oil drilling, but in recent years, the ever-increasing demand of the world for rare metals continues to drive the development of deep sea mining. Therefore, this thesis focuses on the deep sea mining within the Norwegian interest zone along the North-East part of the Mid-Atlantic Ridge outside Svalbard, where the water depth is in excess of 3000 m. The related knowledge of mining is shown in this section.

2.2.1. Mining minerals

The traditional interests of minerals are in Ni-Cu-Mn for nodules, Co-Ni-Mn for crusts, and Cu-Zn-Au-Ag for seafloor massive sulfides (SMS). In addition, research shows that there are additional precise and rare-earth elements (REEs) as potential bi-products of major metal minerals.. For instance, nodules also have high concentrations of Co, Li, Mo, REEs, Y, and Zr in addition to the main metals of interest; crusts have significant concentrations of Bi, Mo, Nb, Pt, REEs, Te, Th, Ti, W, Y, and Zr; and sulfides in some environments, especially volcanic arcs, may have high concentrations of As, Cd, Ga, Ge, In, Sb, and/or Se [5].

Fe-Mn Crusts

Fe-Mn crusts precipitates from the bottom waters of the cold environment (hydrological geology) to the surface of seamounts, ridges, and plateaus as pavements and coatings on rocks in the areas that are kept sediment-free for millions of years. Crusts are usually found at water depths of 400 -7000 m, as well as the thickest and most metal-rich crusts occurring at depths of about 800-2500 m. The distribution of crusts and characteristics of sea mounts indicate that mining operations may be performed at water depths from about 1500 to 2500 m[5].

Fe-Mn nodules

Fe-Mn nodules can be found throughout the global ocean, predominantly on the surface of sediment-covered abyssal plains at water depths of around 3500 to 6500 m. Some nodules are partly buried in the sediment and others are completely buried. The most wide-ranging deposits have been found in the Pacific Ocean, especially between the Clarion and Clipperton Fracture Zones (CCZ), the Peru Basin, and Penrhyn-Samoa Basins[5].

Seafloor massive sulfide (SMS)

Seafloor Massive Sulfide (SMS), sediments are areas of hard substratum with high base metal and sulfide content which are formed by the hydrothermal circulation

and are frequently found at hydrothermal vent sites. It has high base metal content, as well as commercially exploitable concentrations of gold and silver[6]. The most of the deposits of SMS are at water depths of approximately 1400 to 4000m[6]. Moreover, up to 40% of the known deposits occur at shallower depths ≤ 2 km in back-arc basins and on submarine volcanic ridges within 200 nautical miles of the coast and within the jurisdiction of national exclusive economic zones (EEZs)[7].

Based on the follow details, the seafloor massive sulfides (SMS) are more potential to exploit around 3000m.

2.2.2. Mining system

Refer to the mining case of Solwara 1[7], which sites in the Manus Basin off Papua New Guinea is to crush the ore on the seabed. From Figure2-1, it can be found that the mining system mainly contains the mining support vessel, riser and lift system, pump and seafloor mining tool. In this thesis, the model was simplified into the top of riser was connected to the vessel and the end of the riser was connected to the pump. Therefore, the flexible jumper between the pump and the seafloor mining tool was not considered during the analysis.

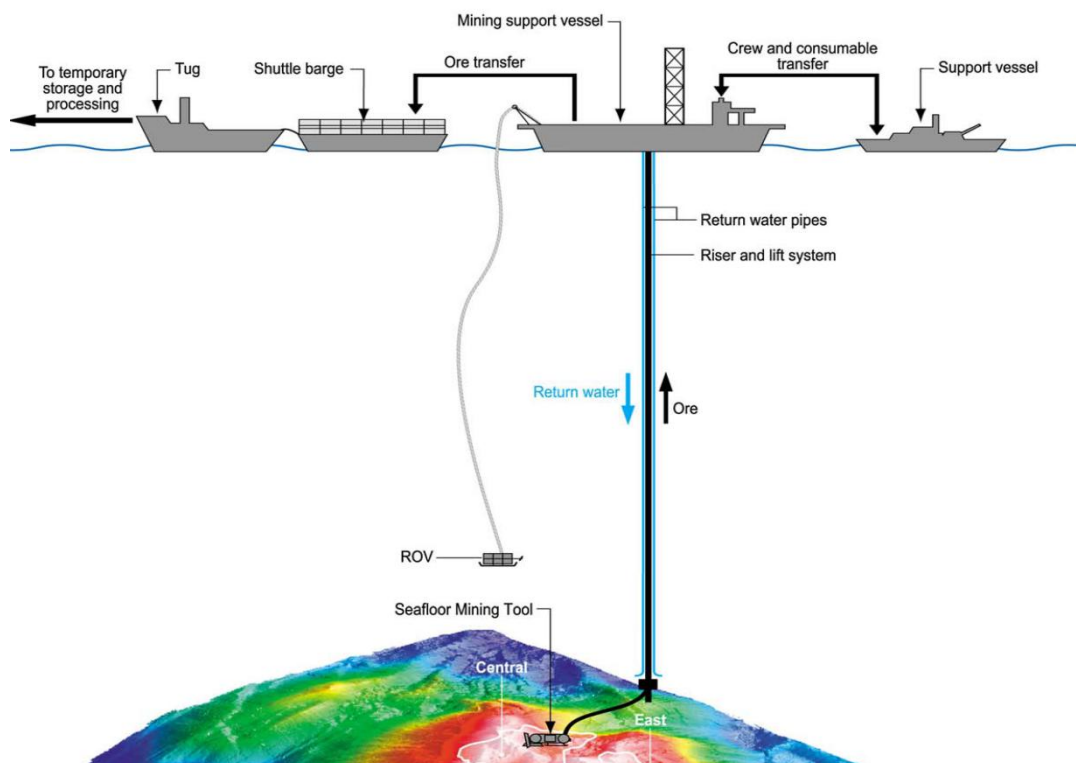


Figure 2-1. Schematic of SMS mining technology and plan for the Solwara 1 deposit off Papua New Guinea[7]

2.2.3. Mining support vessel

In the Section 2.1, the importance of the motion characteristics of the vessel which is connected with the riser has been mentioned. Therefore, the selection of the mining support vessel is very significant.

Related paper reports that the Nautilus Company, will use the vessel as a floating base for its subsea mining operations at the Solwara-1 project located in the Bismarck Sea, offshore Papua New Guinea (PNG). It will extract copper, gold, silver and ore from the seabed at water depths of 1,600m. MAC will own and provide marine management services for the vessel[8]. The estimated parameters of the ship can be seen in Table 2-1. The model for the world's first seabed mining vessel can be seen in Figure 2-2.

Table 2-1. The parameter of the example ship[8]

Length overall	227m
Breadth	40m
Depth	14m
Draft(full loaded)	8.5m



Figure 2-2. The model for the world's first seabed mining vessel[8]

3. DNV GL rules and regulations

The relevant standards and rules related to riser design have been selected based on the framework of DNV GL must be met. The standards and rules are related to the loads and limit states of the riser.

3.1. DNV-OS-F201: Dynamic risers

DNV-OS-F201 (2010)[9] provides criteria, requirements and guidance on structure design and analysis of riser systems exposed to static and dynamic loading for use in the offshore petroleum and natural gas industries. Even if this thesis is focused on the offshore mineral industries, the basic standards are totally sufficient to be referenced .

3.1.1. Loads

Before getting the response of the riser in the 3000m deep water during the different sea states, the first aim is to figure out the loads of the riser.

Section 3 in DNV-OS-F201 (2010) defines the loads to be considered in the design of riser systems. Loads and deformations are categorised into four groups as follows:

- Pressure loads;
- Functional loads;
- Environment loads;
- Accident loads.

Combined with the analysis requirements of the riser, the pressure loads, functional loads and environmental loads are essential. Accidental loads were not considered in this study. The definition of these loads are shown as follows.

Pressure (P) loads are loads that are strictly due to the combined effect of hydrostatic internal and external pressure. The internal pressure definitions apply at the surface (top) of the riser can be divided into design pressure and incidental pressure. Design pressure is the maximum surface pressure during normal operations. Moreover, incidental pressure is the surface pressure that is unlikely to be exceeded during the life of the riser.

Functional (F) loads are defined as loads that occur as consequence of the physical existence of the system and by operating and handling of the system , without environmental or accident load.

In this study, weight and buoyancy of riser, coating, buoyancy modules and pump; weight of internal minerals; applied tension for top-tension risers; installation induced residual loads or pre-stressing are relevant.

Environment (E) loads are loads imposed directly by the ocean environment. The principle environmental parameters are wave, currents and floater motions.

In this study, wave (different sea states, containing extreme condition); current; floater motions induced by waves and current are relevant.

3.1.2. Design criteria for riser pipes

Section 5 in DNV-OS-F201 (2010) provides the general framework for design of riser systems including provisions for checking of limit states for pipes in riser systems.

The limit states are grouped into the following four categories:

Serviceability Limit State (SLS) requires that the riser must be able to remain in service and operate properly. This limit state corresponds to criteria limiting or governing the normal operation (functional use) of the riser;

Ultimate Limit State (ULS) requires that the riser must remain intact and avoid rupture, but not necessary be able to operate. For operating condition this limit state corresponds to the maximum resistance to applied loads with 0.01 annual exceedence probability;

Accidental Limit State (ALS) is a ULS due to accidental loads (i.e. infrequent loads)

Fatigue Limit State (FLS) is an ultimate limit state from accumulated excessive fatigue crack growth or damage under cyclic loading.

This study attempts to find the limit sea states for the riser by the dynamic analysis. Then finding the life time of the riser as a result of the different sea states. Therefore, ultimate limit state and fatigue limit state is considered here.

The typical limit states of ULS for the riser system are as follows:

- **Bursting:** Membrane rupture of the pipe wall due to internal overpressure only.
- **Hoop buckling (collapse):** Gross plastic deformation (crushing) and/or buckling (collapse) of the pipe cross section caused by external overpressure only.
- **Propagating buckling:** Propagating hoop buckling initiated by hoop buckling.
- **Gross plastic deformation, local buckling and hoop buckling:** Gross plastic deformation and hoop buckling of the pipe cross section and/or local buckling of the pipe wall due to the combined effect of external overpressure, effective

tension and bending moment.

- **Unstable fracture and gross plastic deformation:** Unstable crack growth or rest ligament rupture or cross section rupture of a cracked component.
- **Liquid tightness:** Leakage in the riser system including pipe and components.
- **Global buckling:** Overall column buckling (Euler buckling) due to axial compression (negative effective tension).

In this study, due to the overpressure is so small, it was neglected during the analysis.

3.1.3. Combined loading criteria of ULS

Section 5 in DNV-OS-F201 (2010) gives the combined loading criteria of ULS:

Pipe members subjected to bending moment, effective tension shall be designed to satisfy the following equation:

$$\gamma_{sc} * \gamma_m * \left\{ \frac{|M_d|}{M_k} + \left(\frac{T_d}{T_k} \right)^2 \right\} \leq 1 \quad (3-1)$$

Where:

M_d is the design bending moment;

T_d is the design effective tension;

M_k is the (plastic) bending moment resistance given by :

$$M_k = f_y * \alpha_c * (D - t)^2 * t \quad (3-2)$$

T_k is the plastic axial force resistance given by:

$$T_k = f_y * \alpha_c * \pi * (D - t) * t \quad (3-3)$$

f_y is the yield strength to be used in design;

α_c is the flow stress parameter accounting for strain hardening;

D is the riser outer diameter;

t is the riser thickness;

γ_{sc} is the safety class resistance factor, which shown in Table3-1;

γ_m is the material resistance factor, which shown in Table3-2;

Table 3-1. The safety class resistance factor

<i>Low</i>	<i>Normal</i>	<i>High</i>
1.04	1.14	1.26

Table 3-2. The material resistance factor

<i>ULS & ALS</i>	<i>SLS & FLS</i>
1.15	1.0

3.2. DNV-OS-F204: Riser fatigue

DNV-OS-F204 (2010)[10] aims to outline the methodology for performing fatigue assessment of metallic risers subjected to cyclic loads.

The objective of fatigue design is to ensure that the risers have adequate fatigue life. Calculated fatigue lives also form the basis for efficient inspection programmes during fabrication and operational life of the risers.

There are two methods of fatigue assessment, one is using S-N curves, the other one is by crack propagation calculations. The method of using S-N curves is more well-developed and was therefore here.

When using the assessment methods based on S-N curves, the following steps shall be considered:

- assessment of short-term distribution of nominal stress range ;
- selection of appropriate S-N curve ;
- incorporate thickness correction factor;
- determination of stress concentration factor (SCF) not included in the S-N curve;
- determination of accumulated fatigue damage over all short term conditions.

Standard design fatigue factors

The standard DFF is applicable to traditional riser concepts known to have adequate reliability. The standard DFF given in Table 3-4 is applicable for steel risers. For the traditional riser concepts, with fatigue limit being the governing criteria and when the calculated fatigue life is close to the target fatigue life, the application of standard DFF needs to be evaluated.

Table 3-3. Design fatigue factors DFF

<i>Low</i>	<i>Normal</i>	<i>High</i>
3.0	6.0	10.0

3.3.DNV-OS-C203: Fatigue design of offshore steel structures

DNV-OS-C203 (2011)[11] provides more details on the S-N curves and how to select the appropriate S-N curves.

The basic design S-N curve is given as:

$$\log N = \log \bar{a} - m \log \Delta \sigma \quad (3-4)$$

Where:

N is predicted number of cycles to failure of stress range $\Delta \sigma$;

$\Delta \sigma$ is stress range;

$\log \bar{a}$ is intercept of log N -axis by S-N curve;

m is negative inverse slope of S-N curve.

Based on the standards in DNV-OS-C203, the E curve was selected for the fatigue analysis of the riser. In the E curve, the negative inverse slope is 3.0, the intercept of log N-axis is 11.61 . The reason for choosing E curve is as follow:

- **Transverse butt welds, welded from both side:** Transverse splices in plates, flats, rolled sections or plate girders made at site. The height of the weld convexity not to be greater than 20% of the weld width. Weld run-off pieces to be used and subsequently removed, plate edges to be ground flush in direction of stress.
- **Hollow sections :** Circumferential butt weld made from both sides made at site.The applied stress must include the stress concentration factor to allow for any thickness change and for fabrication tolerances.
- **Detailed relating to tubular members (continued):** Parent material (of the stressed member) adjacent to the toes of a bevel butt or fillet welded attachments in region of stress concentration.

4. Non-linear time domain analysis

Non-linear analysis is needed when there is a nonlinear relation between the force applied to the structure and the the response. Nonlinear effects can originate from geometrical nonlinearity (i.e.large deformation), material nonlinearity (i.e. elasto-plastic material), contact[12] and non-linear loads where the latter is most important in this study, represented by the quadratic drag force.

The SINTEF computer program SIMA[13] was used to simulate the structural response of riser in the various sea states. In SIMA, the non-linear static analysis method coupled to a time domain dynamic analysis procedure where all relevant nonlinearities are included. This section gives a brief description of the method applied in SIMA.

4.1. Finite elements formulations

The structural analysis part of the RIFLEX program is based on finite element modelling where the structure is represented by a finite number of elements. Then the equations established for the finite elements are assembled into a large system of equations to simulate the whole structure.

In this case, beam elements were used. The beam element is formulated using the concept of co-rotated ghost reference as outlined in Fundamental Continuum Mechanics Theory[14]. As indicated in Figure4-1, the beam has 3 translational and 3 rotational degrees of freedom at each node. They are defined in relation to the local x, y, z -system in the C_{0n} configuration[15].

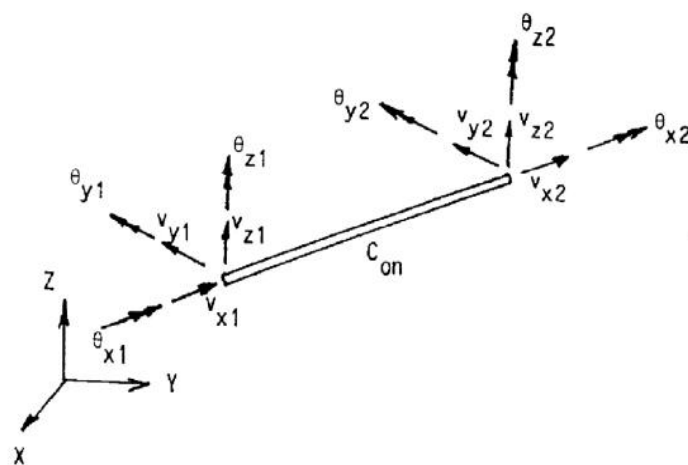


Figure 4-1. Nodal degrees of freedom for beam element[15]

The incremental static equilibrium[16] equation can be defined as:

$$\Delta R = (K_m + K_\sigma) \Delta r \quad (4-1)$$

Where:

ΔR is the element force vector;

K_m is the material stiffness matrix;

K_σ is the initial stiffness matrix;

Δr is the element nodal displacement vector.

4.2. Load models

Based on the Section 3.1.1, for external loads, it is known that the static or quasi-static response results from the current loads, and the dynamic response due to the wave loads as well as the resulting vessel motion loads. These loads are presented in details as follows.

4.2.1. Hydrodynamic loads

To calculate current or wave loads, an extended form of Morison's equation has been used. Morison's equation was originally formulated for calculating the wave loads on fixed vertical cylinders. There are two force components; one is related to water particle acceleration (the inertial force) and the other related to water particle velocity (the drag force)[17].

The extended form of Morison's equation is:

$$F_w = (m \cdot a_w + C_A \cdot m \cdot a_r) + \frac{1}{2} \rho V_r |V_r| C_D A \quad (4-2)$$

Where:

F_w is the fluid force;

m is the mass of fluid displaced by the body;

a_c is the fluid acceleration relative to earth;

C_A is the added mass coefficient for the body;

a_r is the fluid acceleration relative to the body;

ρ is the density of water;

V_r is the current velocity relative to the body;

C_D is the drag coefficient;

A is the drag area.

The term in parentheses is the inertia force, and the other is the drag force. In the riser analysis, C_D varies between 0.7 and 1.2[17].

4.2.2. Wave kinematics

In this case, irregular wave time domain analysis was applied. Based on the linear wave theory, the wave kinematics is generated from a wave spectrum, either in terms of $S(\omega)$ being a function of the frequency alone for long-crested waves or in terms of $S(\omega, \theta)$ being a function of frequency and direction for short-crested waves[18].

In order to generate a time series representation of the sea state, the phases are randomly selected from a uniform distribution, with the amplitude of Fourier components fixed by a filtered power spectrum. The resulting wave elevation is then as a sum of linear waves and identified as the first order contribution in the perturbative expansion of η [18].

The relationship between the $S(\omega)$ and η can be expressed as:

$$S(\omega)d\omega = \frac{1}{2}\eta^2 \quad (4-3)$$

$$\eta = \sum \sqrt{2S(\omega)\Delta\omega} \cos(\omega t + \theta) \quad (4-4)$$

And $\eta(t)$ is the wave elevation as a function of time. When $\eta(t)$ is defined, the kinematic velocities and accelerations along the riser are obtained using linear wave theory.

After defining the spectrum, the seed for generation of random phase angles must be specified. With different seed numbers, different realisations of the wave time series will be generated.

In this case, JONSWAP spectrum was selected from the irregular wave package of SIMA. The details of the JONSWAP spectrum[19] are shown below.

$$S_{\zeta}(\omega) = \frac{\alpha g^2}{\omega^5} \exp\left(-\beta\left(\frac{\omega_p}{\omega}\right)^4\right) \gamma^{\exp\left(\frac{(\frac{\omega}{\omega_p}-1)^2}{2\sigma^2}\right)} \quad (4-5)$$

The wave spectrum contains the following parameters:

ω_p is the peak frequency, $\omega_p = \frac{2\pi}{T_p}$, T_p is the peak periods;

α is the spectrum parameter;

γ is the peakedness parameter;

β is the form parameter, default value is 1.25;

σ is the spectral parameter with default values. $\sigma = 0.07$ if $\omega \leq \omega_p$, $\sigma = 0.09$ if $\omega \geq \omega_p$.

Significant wave height H_s is often used instead of α to parameterize the spectrum:

$$\alpha = \left(\frac{H_s \omega_p^2}{4g} \right)^2 \frac{1}{0.065\gamma^{0.803} + 0.135} \quad (4-6)$$

Another formula giving the same α is:

$$\alpha = 5.061 \frac{H_s^2}{T_p^4} (1 - 0.287 \ln(\gamma)) \quad (4-7)$$

Eq. (4-6) and Eq. (4-7) have been implemented in the program as alternative to specifying α , γ may normally be taken as:

$$\gamma = \exp \left[3.484 \left(1 - 0.1975 \delta \frac{T_p^4}{H_s^2} \right) \right] \quad (4-8)$$

$$\delta = 0.036 - 0.0056 \frac{T_p}{\sqrt{H_s}}$$

However, for a two parameter JONSWAP spectrum, the following limits on γ are valid:

$$T_p \geq 5\sqrt{H_s} \quad \gamma = 1.0$$

$$T_p \leq 3.6\sqrt{H_s} \quad \gamma = 5.0$$

4.2.3. Vessel motion

The top of the riser was attached to a vessel, using the response amplitude operator (RAO) including the first and second order motion of the vessel as the vessel loads on the riser. Generation of motion time series will be consistent with generated time series for wave-induced water particle velocities and accelerations. The rigid body motion responses consist of 6 degrees of freedom: surge, sway, heave, roll, pitch and yaw referred to the global (X Y Z) coordinate system.

The motion model consists of a set of high-frequency (wave frequency) motions in all 6 degrees of freedom and a set of low-frequency motions in the 3 horizontal degrees of freedom: surge, sway and yaw. These two sets of motions are referred to as HF-motions and LF-motions, respectively. For most dynamic line problems it is sufficient to include only the HF-motions. The effects of typical LF-motions, with periods of 60-180 s, can often be covered by suitable selection of static (mean) position.

4.3. Analysis procedure

There are three steps in the analysis process. The first step is static analysis, and then the wave load is applied on the structure to proceed the dynamic analysis.

4.3.1. Static analysis

The aim of static analysis is to determine the initial static geometry of the riser configuration. The design parameters to be selected in the static analysis are typically length, weight, buoyancy requirements. The loads considered in the static analysis stage are generally gravity, buoyancy and current loads. [17]

The static analysis is based on the finite element method. The state of the discretized finite element model is completely determined by the nodal displacement vector. The purpose of the static analysis is to determine the nodal displacement vector so that the complete system is in static equilibrium before the onset of the dynamic load. The static equilibrium configuration is therefore found as the solution of the following system of equation[15]:

$$R^I(r) = R^E(r) \quad (4-9)$$

Where:

r is nodal displacement vector including all the degrees of freedom for the system, i.e. displacements for a bar model and displacements and rotations for a beam model. Both displacements and rotations are relative to the stress-free reference

configuration.

$\mathbf{R}^I(\mathbf{r})$ is internal structural reaction force vector found by assembly of element contributions. Contact forces are also treated as internal reaction forces.

$\mathbf{R}^E(\mathbf{r})$ is external force vector assembled from all elements. Accounts for specified external forces, rigid body forces for representation of buoys, pump weights etc. and contribution from distributed loading, i.e. buoyancy and current forces.

Moreover, the equation of the finite element should be solved by iteration. The Newton-Raphson method is the most frequently used iterative method for solving non-linear structural problems.

In details, the Newton-Raphson method[16] is presented below:

The Newton-Raphson algorithm to solve x for the problem $f(x)=0$ is

$$x_{n+1} = x_n - \frac{f(x_n)}{f'(x_n)} \quad (4-10)$$

Where $f'(x_n)$ is the derivative of $f(x)$ with respect to x , at $x = x_n$.

In this study, $\mathbf{K}(\mathbf{r})d\mathbf{r} = d\mathbf{R}$, \mathbf{K}_I is the incremental stiffness matrix, which represents the generalisation of the $\partial f / \partial x$. \mathbf{r} is the displacement vector and \mathbf{R} is the load vector.

In Newton's method for a single dof $\frac{\partial \mathbf{r}}{\partial f(\mathbf{r})} = -\mathbf{K}_I^{-1}(\mathbf{r}_n)$,

The equation: $f(\mathbf{r}) = \mathbf{R} - \mathbf{R}_{int} = 0$ is solved by the iteration formula:

$$\mathbf{r}_{n+1} - \mathbf{r}_n = \delta \mathbf{r}_{n+1} = \mathbf{K}_I^{-1}(\mathbf{r}_n)(\mathbf{R} - \mathbf{R}_{int}) \quad (4-11)$$

4.3.2. Dynamic analysis

As the dynamic performance of the riser is non-linear, the results of the frequency domain analysis can not be accurate. Therefore time domain analysis is commonly used to analyze the performance of the riser. The starting point for dynamic simulation is the static equilibrium configuration. The dynamic analysis primarily represents the analysis of the riser response to the combined action of the wave and current. Then the dynamic simulation considers the RAO of the vessel over a

specified period of time. The RAO is used to represent the motion of the vessel, which acts as the loading at the top of the riser, and then to carry out the dynamic analysis. [17]

Then the method of analysis used in nonlinear dynamic analysis will be introduced. The presentation mainly follows the approach outlined by Remseth (1978) [20] The nonlinear incremental equation of motion is linearized by introducing the tangential mass-, damping- and stiffness matrices at the start of the increment. The linearized incremental equation of motion can be expressed as:

$$\mathbf{M}_t \Delta \ddot{\mathbf{r}}_t + \mathbf{C}_t \Delta \dot{\mathbf{r}}_t + \mathbf{K}_t \Delta \mathbf{r}_t = \Delta \mathbf{R}_t^E \quad (4-12)$$

Where \mathbf{M}_t , \mathbf{C}_t and \mathbf{K}_t denote the tangential mass-, damping- and stiffness matrices computed at time t. $\Delta \mathbf{r}_t$, $\Delta \dot{\mathbf{r}}_t$, $\Delta \ddot{\mathbf{r}}_t$ and $\Delta \mathbf{R}_t^E$ are the incremental displacement, velocity, acceleration and external force vectors, respectively.

$$\begin{aligned} \Delta \mathbf{r}_t &= \mathbf{r}_{t+\Delta t} - \mathbf{r}_t \\ \Delta \dot{\mathbf{r}}_t &= \dot{\mathbf{r}}_{t+\Delta t} - \dot{\mathbf{r}}_t \\ \Delta \ddot{\mathbf{r}}_t &= \ddot{\mathbf{r}}_{t+\Delta t} - \ddot{\mathbf{r}}_t \\ \Delta \mathbf{R}_t^E &= \mathbf{R}_{t+\Delta t}^E - \mathbf{R}_t^E \end{aligned} \quad (4-13)$$

Due to nonlinearities, the dynamic equilibrium equation is not satisfied at the end of the time step. The residual force vector, due to change in mass, damping and stiffness over the time step is given by:

$$\delta \mathbf{R}_t = \mathbf{R}_{t+\Delta t}^E - (\mathbf{R}_{t+\Delta t}^I + \mathbf{R}_{t+\Delta t}^D + \mathbf{R}_{t+\Delta t}^S) \quad (4-14)$$

Where:

- \mathbf{R}^I is inertia force vector;
- \mathbf{R}^D is damping force vector;
- \mathbf{R}^S is internal structural reaction force vector;
- \mathbf{R}^E is external force vector.

To prevent error accumulation, the residual force vector is added to the incremental equilibrium equation at the next time step. Thus, the incremental equation of motion including equilibrium correction is written as:

$$\mathbf{M}_t \Delta \ddot{\mathbf{r}}_t + \mathbf{C}_t \Delta \dot{\mathbf{r}}_t + \mathbf{K}_t \Delta \mathbf{r}_t = \mathbf{R}_{t+\Delta t}^E - (\mathbf{R}_t^I + \mathbf{R}_t^D + \mathbf{R}_t^S) \quad (4-15)$$

Then the incremental equation expressed by the incremental displacement vector over the time interval $[t, t + \Delta t]$, is written as:

$$\hat{\mathbf{K}}_t \Delta \mathbf{r}_t = \Delta \hat{\mathbf{R}}_t \quad (4-16)$$

Where \hat{K}_i is the effective stiffness, $\Delta\hat{R}_i$ is the effective incremental load vector.

Finally, to obtain dynamic equilibrium at the end of the time step, an iterative approach similar to the static equilibrium iteration by the Newton-Raphson method is applied.

4.3.3. Fatigue analysis

Fatigue damage is caused by cyclic stresses. Due to cyclic stresses, the material slowly undergoes plastic deformation which first lead to cracks and can eventually lead to fatigue. It is important to ensure that the riser has adequate fatigue life is very significant. The steps for the fatigue calculation are presented in Figure4-2 .

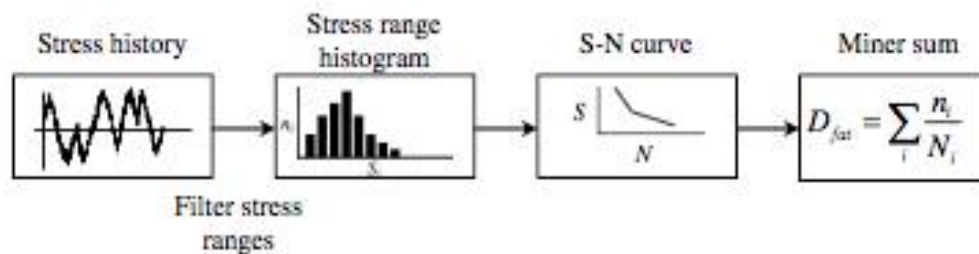


Figure 4-2. The fatigue analysis procedure.

A general approach for calculation of wave and low frequency fatigue damage contributions is based on application of the following procedure:

The first step is to implement the environment (sea states) data. The wave environment scatter diagram is subdivided into a number of representative blocks. Within each block, a single sea-state is selected to represent all the sea-states within the block. The probabilities of occurrence for all sea-states within the block are lumped to the selected sea-state. The fatigue damage is computed for each selected short term sea-state for all the blocks [9].

The weighted fatigue damage accumulation from all sea states can be expressed as:

$$D_L = \sum_{i=1}^{N_S} D_i P_i \quad (4-17)$$

Where:

D_L is long-term fatigue damage;

N_S is number of discrete sea states in the wave scatter diagram;

P_i is sea state probability. Normally parameterised in terms of significant wave height and peak period, i.e. $P(H_s, T_p)_i$;

D_i is short term fatigue damage.

The second step of fatigue analysis is to define the fatigue loading. This can obtained

from the results of the dynamic analysis of the different sea states. In this case, the fatigue stress is the resultant axial stress, which contains bending moment stress and axial tension stress. Then identifying the locations to be assessed, i.e. which locations have the highest axial stresses. Moreover, for the riser, after finding the hot spot location, 8 points on the cross section is considered.

After that, based on the dynamic analysis results (forces and moments) from SIMA, using rainflow counting method to obtain the time history of the stress. Then rearranging the stress history into blocks, and getting the stress range histogram. Moreover, identifying the fatigue strength data, which is the S-N curves from DNV rules. From Section 3, it is known that the E curve has been selected.

Then considering the influence of a thickness correction factor to the nominal stress range:

$$S = s_0 * SCF * \left(\frac{t_3}{t_{ref}}\right)^k \quad (4-18)$$

Where:

s_0 is nominal stress range;

SCF is stress concentration factor;

$\left(\frac{t_3}{t_{ref}}\right)^k$ is thickness correction factor.

The thickness correction factor applies for pipes with a wall thickness t_3 greater than a reference wall thickness, $t_{ref}=25\text{mm}$. However, in this study, the thickness of the riser is 15mm. Therefore, there is no need to consider this correction.

Finally, the Miner-Palmgren rule is adopted for accumulation of fatigue damage from stress cycles with variable range:

$$D = \sum_i \frac{n(S_i)}{N(S_i)} \quad (4-19)$$

Where $n(S_i)$ is the number of stress cycles with range S_i , and $N(S_i)$ is the number of stress cycles to failure.

5. Modelling by SIMA

The riser system is modeled in SIMA to evaluate its dynamic behaviour under the various sea states with regard to two working conditions and to figure out the limiting sea states. The two working conditions, one is the operating condition, riser is during the procedure of transporting the minerals from the seabed to the vessel, in this situation, the top of the riser is connected to the vessel by a pin joint. Another is the installing condition, under which condition, the top of riser is fixed to the vessel.

Based on the lumped mass method, the riser is modeled as a line, which is divided into a series of line segments. The line segments only model the axial and torsional properties of the line. The other properties (mass, weight, buoyancy, etc.) are all lumped to the nodes.[17] In this model the water depth is 3000m, and the riser length is 2970m. It means from the end of riser to the seabed is still 30 meters long. The end of the riser is connected with a pump. The pump is connected to the mining equipment on the seabed by another section of flexible jumper. However, in this case, the section below the pump is not considered. The model can be seen in Figure5-1 .

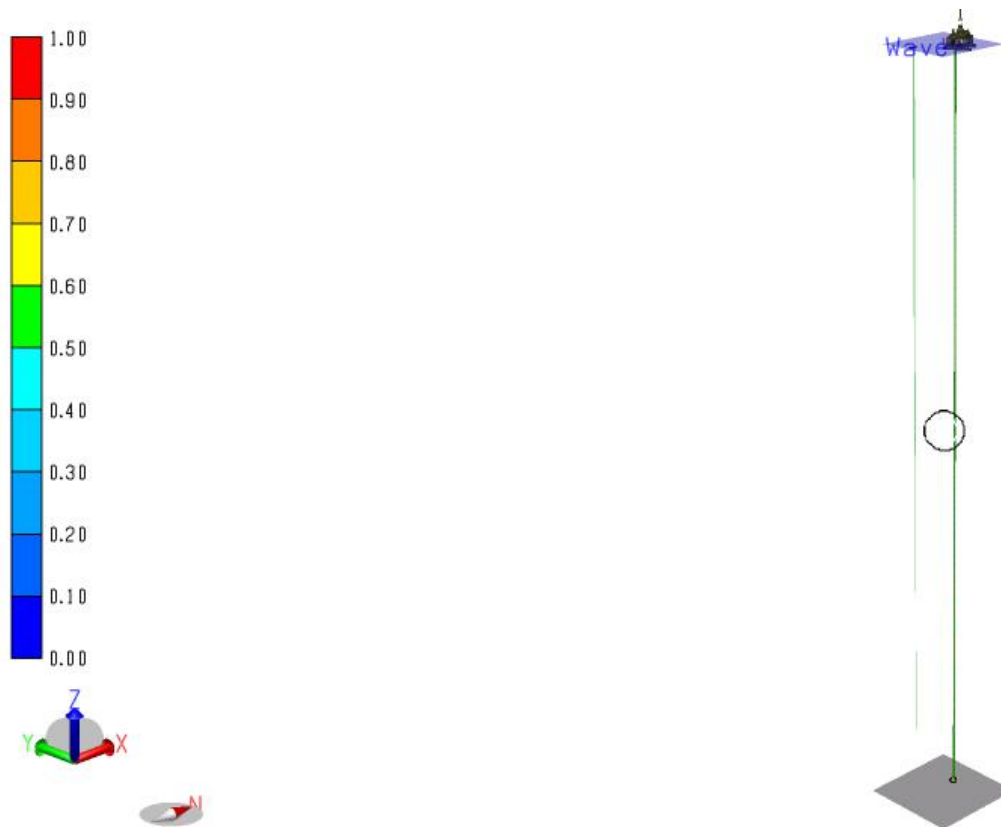


Figure 5-1. The riser model from SIMA.

5.1. The environment condition

The environment defines the conditions which the riser lift model are operated in. In this study, the marine environment of the place along the North-East part of the Mid-Atlantic Ridge outside Svalbard will be simulated as real as possible.

The operating water depth is 3000m, while the influence by the change of tide has not been considered. The current velocity on the free surface was set to 0.5m/s. It has a linear inverse relationship with water depth. As the water depth increases, the current velocity decreases to zero, as shown in Figure5-2 .

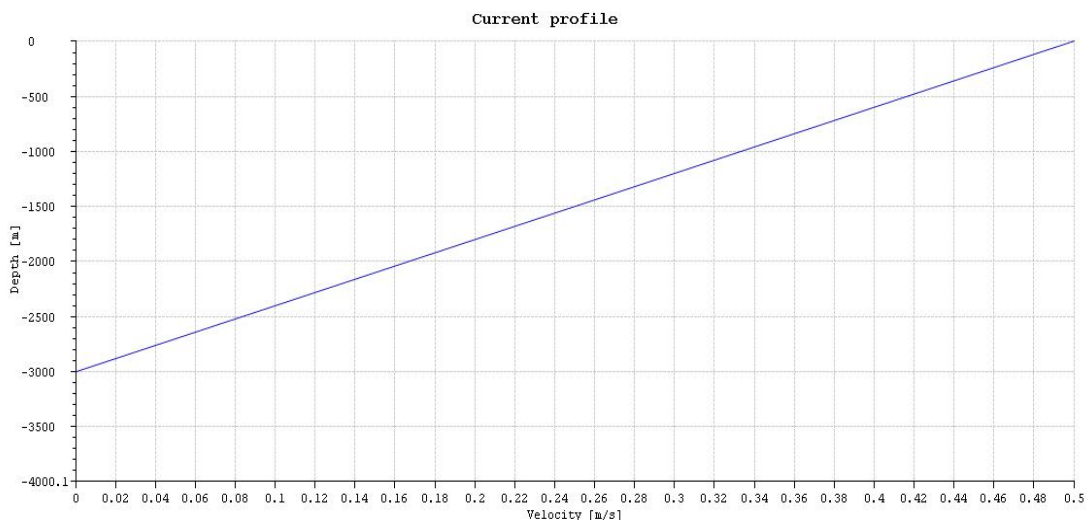


Figure 5-2.The relationship between the current velocity and the water depth.

Jonswap-3Parameter spectrum was selected. JONSWAP spectrum extends fully-developed sea to include fetch limited seas, describing developing sea states. It describes wind sea conditions that often occur for the most severe sea states[24].

The wave scatter diagram of the northern North Sea was chosen as the sea states that riser will be operated in. Because this scatter diagram is mature and detailed, it has many extreme sea states. Moreover, the wave scatter diagram of the project site which is along the North-East part of the Mid-Atlantic Ridge outside Svalbard will most likely be better than it of the northern North Sea. Therefore, if the riser can be operated under the northern North Sea condition, it can also be operated along the North-East part of the Mid-Atlantic Ridge outside Svalbard. The scatter diagram of the northern North Sea is shown in Figure5-3 .

And the wave spectrum of one of the sea states (H_s is 4m and T_p is 8s) is presented in Figure5-4 .

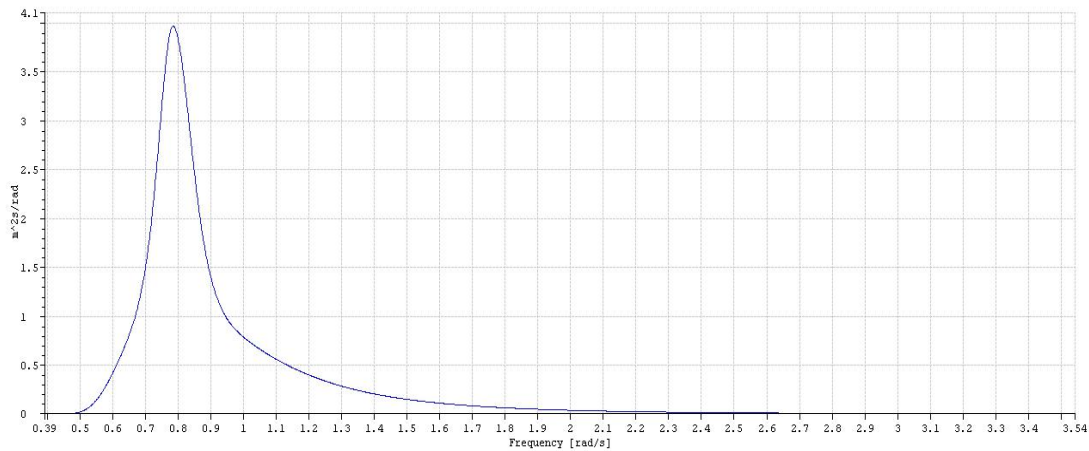


Figure 5-4. The wave spectrum of the significant on H_s is 4m and T_p is 8s.

5.2. Riser system

The definition terms of the simplified riser system are presented in the Figure5-5 .

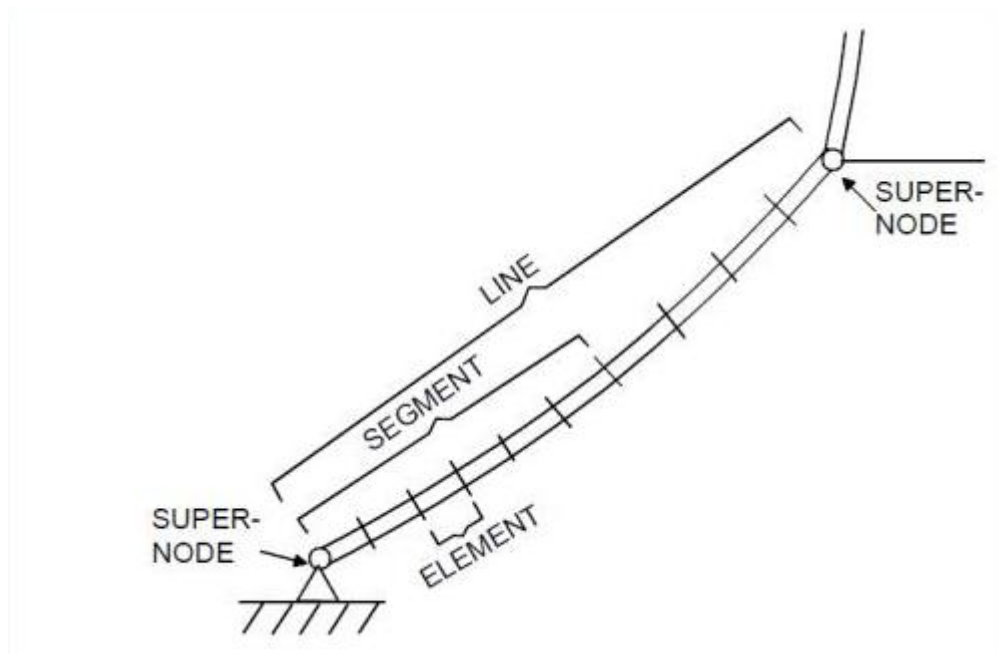


Figure 5-5. Riser system definition terms.

Supernode: Branching points or nodes with specified boundary conditions

Line: Suspended structure between two supernodes

Segment: (Part of) line with uniform cross section properties and element length

Element: Finite element unit

5.2.1. Boundary condition

There are two working conditions of riser system, which are distinguished by the boundary condition at the top of riser.

In the operating condition, the top of the riser is connected to the vessel by the pin joint. Which means, the connection supernode has six degrees of freedom, all the three components of translation and the rotation of Z direction are fixed, where the rotation of X and Y direction are free. In details, the boundary condition frame is relative to the vessel and X, Y, Z-direction is under the global coordinate system.

In addition, in the installation condition, all six degrees of freedom of the connection are fixed. It means the top of the riser is both fixed in translation and rotation relative to the vessel.

However, the end of the riser is attached to a pump. When the end of riser was set free to move. The gravity of the pump minus the buoyancy of the pump gives additional tension in the riser.

5.2.2. Riser line types

Just like the structural analysis of a rigid body, the degree of density of the mesh can affect the accuracy of the results. How to divide the line segments and elements of the riser will also affect the accuracy of the results. The division method is shown in Figure5-6 . which means the riser is divided into 3 segments from top to the bottom. Considering that the large deformation of the riser under the Load of current and wave will be at the top of the riser. Therefore the segment 1, the first 30 meter of the riser is divided into 30 elements. Segment 2, is 40 meter long and divided into 16 elements, i.e. each element is 2.5 meters long. For segment 3, the remaining riser of 2900 meter is divided into 580 elements, i.e. each element is 5 meters long. Therefore, there are total 626 elements along the riser.

No	Cross Section	Length	Acc length	Num Elements	El length	Nodal Component
1	axisymmetricPipe	30.0	30.0	30	1.0	
2	axisymmetricPipe	40.0	70.0	16	2.5	
3	axisymmetricPipe	2900.0	2970.0	580	5.0	



Figure 5-6. Riser line types

5.2.3. Components

From Figure 5-6, it is shown that there are two important components in the riser system. One is the nodal body which is connected to the end of the riser, called pump. Another is the internal fluid which flows from the the end of the riser to the top vessel, called mineral.

Pump

The mass of the pump is 90t. The volume of the pump is 28.3 m³, which is assumed as a cylinder. The diameter (D) is 6m, and the height(H) is 1m. The hydrodynamic force coefficient for pump is calculated under the global coordinate system by the following formulas:

The drag force coefficient of the pump in x-direction and y-direction:

$$\frac{1}{2} \rho_w C_D D H = 3075 \text{Ns}^2/\text{m}^2 \quad (5-1)$$

The drag force coefficient of the pump in z-direction:

$$\frac{1}{2} \rho_w \frac{\pi}{4} D^2 = 14490 \text{Ns}^2/\text{m}^2 \quad (5-2)$$

The added mass of the pump:

$$\rho_w C_A V = 28981 \text{ kg} \quad (5-3)$$

The weight loading on the riser provided by the pump is 6*10⁵ N, which was calculated by the weight of pump minus the buoyancy of the pump.

Mineral

The internal fluid that flows in from the bottom of the riser is the slurry flow, which is mixed by the rocks and water. Taking this into consideration, the density of the mineral was set to an upper band value of 2000 kg/m^3 . Since this thesis analyzes the static and dynamic response of the riser during storage and transportation, it is assumed that the mineral is constantly present inside the riser. Therefore, the mineral velocity is zero during the analysis process. Which results in the inlet pressure and the pressure drop of the riser is all zero.

5.2.4. Cross section

The axisymmetric pipe was selected as the riser model, due to the outer layer of the riser needs to be wrapped with buoyant material. The importance of which has been discussed in the Section 2.1. It's worth noting that the local coordinate system (x,y,z) is applied when the related parameters of riser are calculated in this section. The local coordinate system of riser is shown in Figure 5-7.

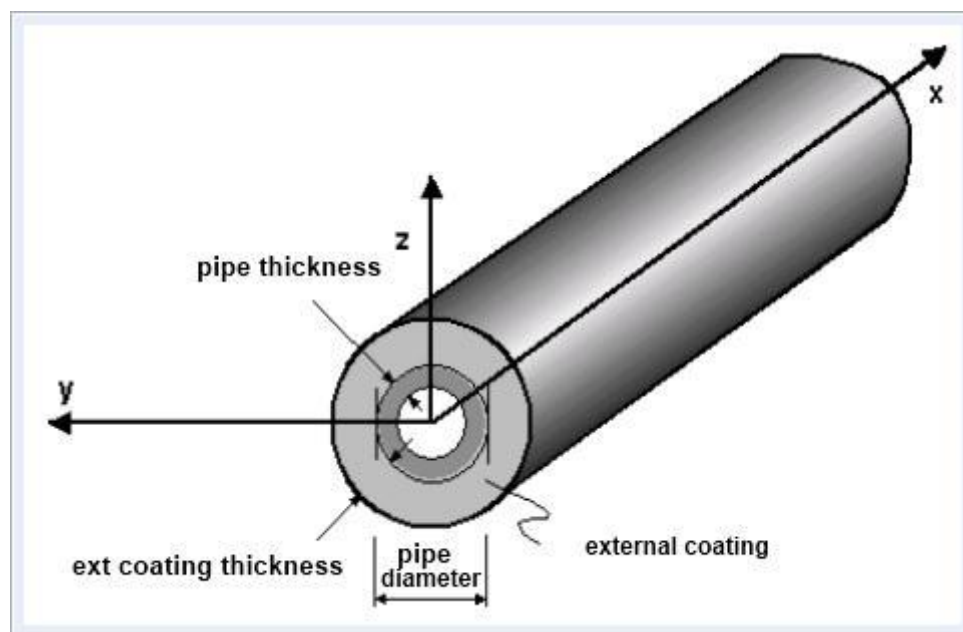


Figure 5-7. The local coordinate system (x,y,z) of riser.

The outside steel pipe diameter was set to 0.3 m and the pipe thickness was set to 0.015m. The pipe material density is 7850 kg/m^3 . Considering the weight of the whole riser model and the pump weight, so the tension of the riser will be large. Therefore, a buoyancy layer was applied outside the steel riser. The density of the buoyancy layer is 600 kg/m^3 . If the total buoyancy provided by the buoyancy layer can completely balance the gravity of the riser, it can be calculated by the buoyancy of the whole riser (contains the buoyancy layer) equaling to the sum of the weight of the steel riser, the weight of the internal mineral and the weight of the buoyancy

layer. Moreover, it is easy to calculate in unit length situation. The follow formula can be used.

$$g(\rho_r \frac{\pi}{4}(D_o^2 - D_i^2) + \rho_m \frac{\pi}{4}D_i^2 + \rho_b \frac{\pi}{4}(D_b^2 - D_o^2)) = \rho_w \frac{\pi}{4}D_b^2 g \quad (5-4)$$

Where:

D_o is the riser overall diameter;

D_i is the riser internal diameter;

D_b is the diameter of the whole riser (contains the buoyancy layer);

ρ_r is the density of riser material (steel);

ρ_m is the mineral density;

ρ_b is the buoyancy layer density;

ρ_w is the density of the sea water, as 1025 kg/m³

g is the acceleration of the gravity.

Based on Eq.(5-4), D_b was calculated to be 0.728m. Then the thickness of the buoyancy layer would be as 0.214m. If this thickness of buoyancy layer is used, the riser weight is totally offset. However, like it has been discussed in the Section 2.1, increasing the thickness of the buoyancy layer will increase the bending moment stress at the top part. Therefore, in order to balance the effects of tension and bending moment, the thickness of buoyancy layer was selected to be 0.05 meter.

Therefore, the weight of the whole riser which contains the inner minerals and outside buoyancy layer is 3.6*10⁶ N.

The cross section properties of the riser can be found in the Figure5-8. And its material properties can be seen in Table5-2.

Axisymmetric Pipe 'axisymmetricPipe' in Simple_Flexible_Riser_irregular

Name: *axisymmetricPipe

Description:

Diameter Type	Pipe Diameter	Pipe Thickness	Material Density	Ext Coating Thickness	Ext Coating Density	Ext Contact Radius	Int Contact Radius
Outer	0.3	0.015	7850.0	0.05	600.0	0.2	0.15

Default Thermal/Pressure Expansion:

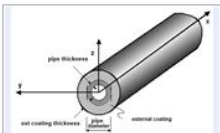


Figure 5-8. The cross section properties of the riser.

The non-dimensional coefficients are selected as the hydrodynamic force coefficient for riser. Moreover, the coefficients are determined under the local coordinate system. So the coefficients of x direction (along the riser) is very small. The specific coefficients of the riser is presented in the Figure5-9.

Cross-section properties | Material properties | Damping specification | **Hydrodynamic force coefficients** | Aerodyn

Load Formulation:

Input code:

Froude Krylov scaling:

Hydrodynamic diameter:

Quadratic drag coefficients:

CQx	CQy
0.05	1.0

Linear drag coefficients:

CLx	CLy
0.0	0.0

Added mass coefficients:

CAx	CAy
0.05	1.0

Figure 5-9. The hydrodynamic force coefficient for riser.

5.3. Support vessels

In some actual operations, the support vessel for the deep sea mining is decided to be FPSO (floating production, storage, and offloading system). Here, the semi-submersible platform was selected to be the support vessel by SIMA package. Both of them, in which production and storage facilities are housed, are appropriate for developing large deposits in deep or ultra deep water. Moreover, they are designed with good stability and seakeeping characteristics. Due to these similarities and advantages, the semi-submersible platform can be the support vessel in this study. The local coordinate system of the semi-submersible platform can be found in Figure5-10.

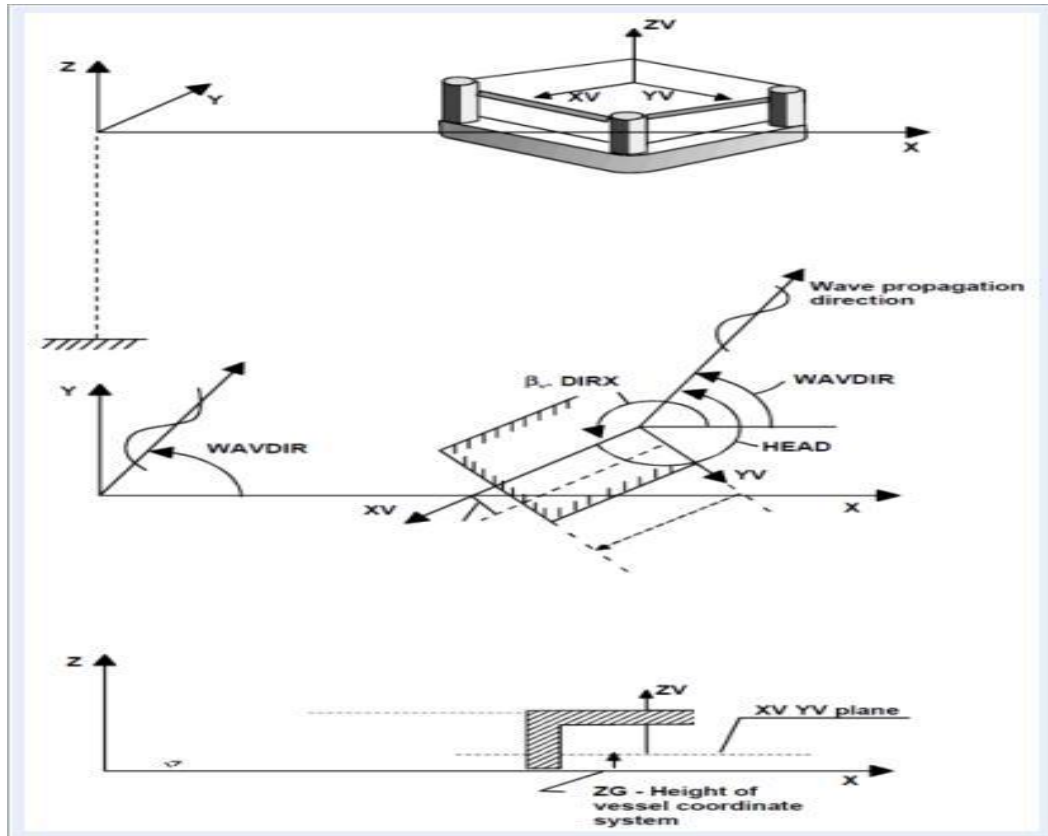


Figure 5-10. The local coordinate system of the semi-submersible platform.

The three degrees of vessel translation motion response amplitude operators (RAOs) are shown in Figure 5-11. And the other three degrees of vessel rotation motion response amplitude operators (RAOs) are shown in Figure 5-12. From these two figures, it can be found when all sea states were applied in the same direction that the main vessel motion will be heave, surge and pitch in this case.

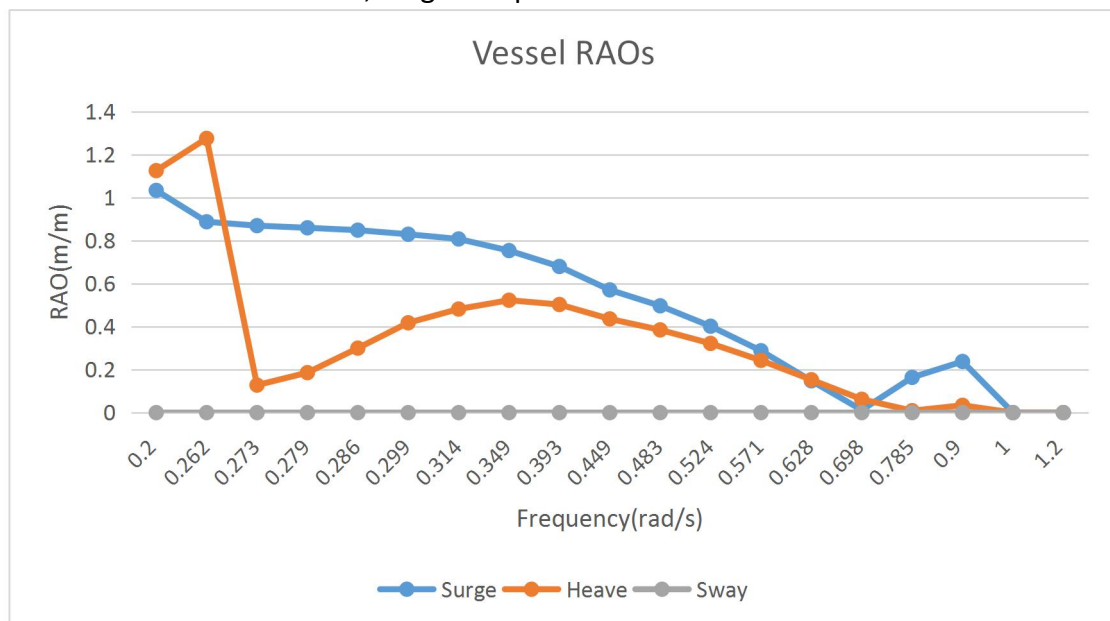


Figure 5-11. The RAOs of vessel translating motion.

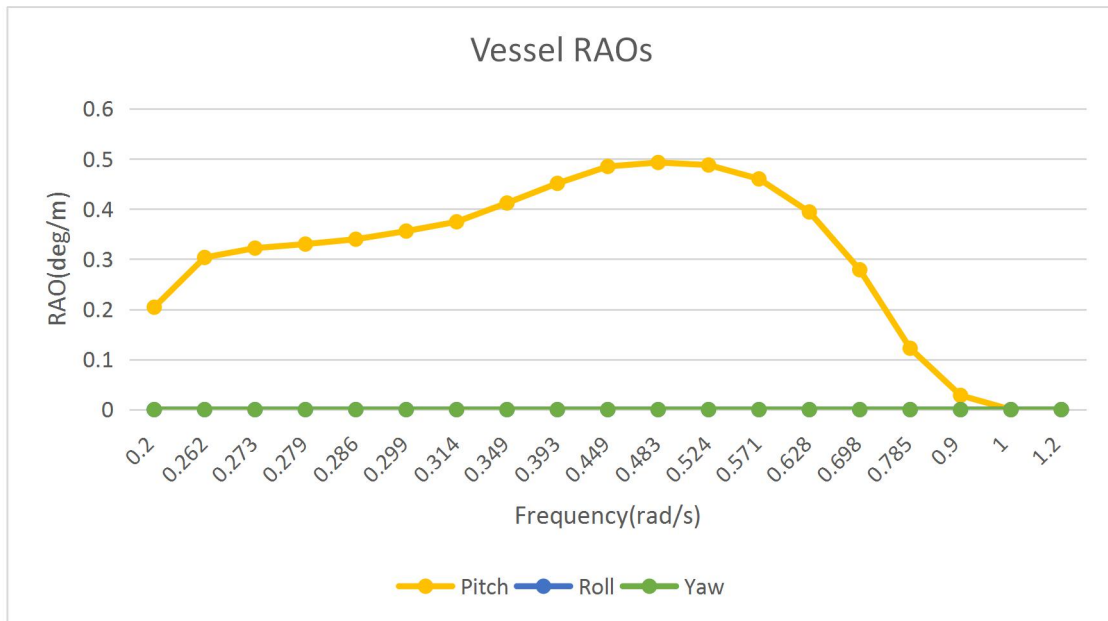


Figure 5-12. The RAOs of vessel rotating motion.

5.4. Static and dynamic calculation parameter

5.4.1. The static calculation parameter

During the static analysis, the riser is loaded by the volume forces, the body forces and the current forces. The matrix storage is sparse, then the load and mass formulation is lumped. The other specific parameter settings is presented in Figure5-13.

Static Calculation in Simple_Flexible_Riser_irregular

Description:

Matrix Storage:

Load And Mass Formulation:

Current Profile Scaling:

Store Visualisation Responses:

Use stress free configuration:

Loading sequence | Load components | Parameter variation

Load Type	Run With Previous	N Step	Max Iterations	Accuracy
Volume Forces	<input type="checkbox"/>	200	20	1.0e-06
Body Forces	<input checked="" type="checkbox"/>	200	20	1.0e-06
Current Forces	<input type="checkbox"/>	200	10	1.0e-06

Figure 5-13. The specific static calculation parameter settings.

5.4.2. The dynamic calculation parameter

During the dynamic analysis, besides the static loading, the riser is also loaded by the wave forces and the resulting vessel motion. The simulation length should be one hour, in case of the instability at the beginning of the operation, the simulation time is extended to 3800s, so the results of the first 200s can be deleted. The other specific parameter settings is presented in Figure5-14.

Dynamic Calculation in Simple_Flexible_Riser_irregular

Description:

Irreg. Analysis | Reg. Analysis | Procedure | Dynamic loads | Storage | HLA

Simulation Length	Time Step
3800.0	0.1

Time series generation parameters

Wave seed
29852

Requested time series length	Time increment	Applied Time Series Length	Frequency Resolution	Number Of Steps
3800.0	0.5	4096.0	0.00024414	8192

Figure 5-14. The specific dynamic calculation parameter settings.

5.5. Input data

The total parameters of the riser lift system has shown before and the related parameters of analysis are arranged into the following Table5-2.

Table 5-2. The total data used in this study.

Water depth	3000m	Total riser length (L)	2970m
Riser overall diameter (D_o)	0.3m	Riser thickness	0.015m
Riser internal diameter (D_i)	0.27m	The Cross-sectional area of riser (A)	0.0134m ²
The density of riser material (ρ_r)	7850 kg/m ³ (steel)	The buoyancy layer thickness	0.05m
Mineral density(ρ_m)	2000 kg/m ³	The buoyancy layer density (ρ_b)	600kg/m ³
Whole riser mass	751t	Riser mass	313t
Pump mass	90 t	Pump volume	28.3 m ³
Elasticity modulus (E)	2.06*10 ¹¹ N/m ²	Shear modulus	8*10 ¹⁰ N/m ²
The total weight loaded on riser	4.2*10 ⁶ N	The weight of pump	6*10 ⁵ N
The weight of whole riser	3.6*10 ⁶ N	Minimum specified yield strength f_y	386 MPa
Flow stress parameter α_c	1.2	Safety class resistance factor γ_{sc}	1.14
Material resistance factor γ_m	1.15	Design fatigue factors DFF	10.0
S-N curves	E curve	Drag coefficient C_D	1.0
Added mass coefficient C_A	1.0	Current velocity on the free surface	0.5 m/s

6. Pinned topside connection analysis results

The operation and installation condition is represented by the pinned topside connection and fixed topside connection, respectively. This section is listed the analysis results for the pinned topside connection. Which means the top of the riser is connected to the vessel by the pin joint. In details, all the three components of translation and the rotation of Z direction are fixed, the rotation of X and Y direction are free.

6.1. Quasi-static analysis

The quasi-static analysis determines the effect of the current only external loading on the riser system. The quasi-static analysis considers the only one current loading condition for the current velocity on the free surface is 0.5m/s. Before the dynamic analysis, the initial static geometry of the riser configuration can be determined by this analysis.

6.1.1. Effective tension

Based on the Section 5, it is known that the total weight loading on the whole riser system is 4.2×10^6 N, among this the weight provided by the pump is 6×10^5 N. From the Figure6-1, it can be found that the effective tension has a linear inverse relationship with the riser length. The effective tension at the top of riser is 4.214×10^6 N, which is experienced by the weight of the whole riser system, as well as the current loading. Moreover, the effective tension at the bottom of the riser is 6.014×10^6 N, which is experienced by the weight of the pump and the current loading.

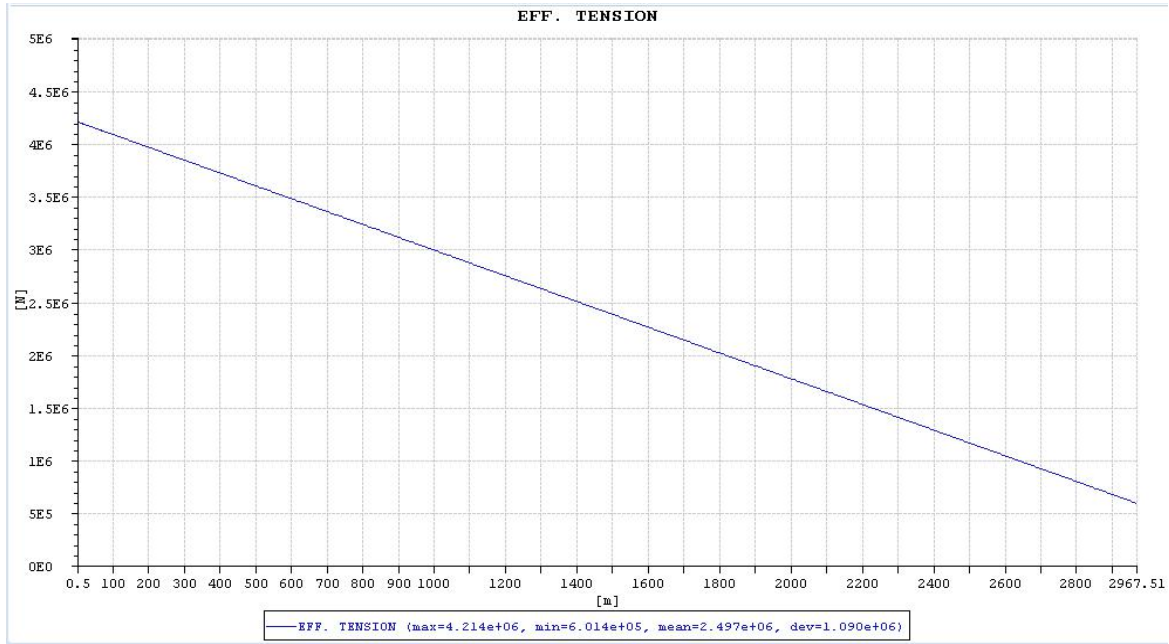


Figure 6-1. The quasi-static effective tension of the riser.

6.2. Eigenfrequency

Based on Figure 6-2, it can be seen when the angular frequency is around 0.9 rad/s, the riser has the biggest response. To explain this phenomenon, the eigenfrequency of the riser should be considered. The eigenfrequency of the first axial mode can be approximated by:

$$\omega_n = \sqrt{\frac{k}{m}} \quad (6-1)$$

Where:

k is the structure stiffness, $k = \frac{EA}{L} = 9.3 \times 10^5 \text{ N/L}$,

m is the structure mass, where m is estimated as the half of the whole riser mass plus the pump mass, which is $4.7 \times 10^5 \text{ kg}$. At this time, this gives a ω_n value of 1.4 rad/s.

Then if the structure mass is estimated as the whole riser mass plus the pump mass, which is $8.4 \times 10^5 \text{ kg}$, ω_n will be around 1.1 rad/s. Therefore, the excitation frequency is always in the range of the axial eigenfrequency of the riser structure in this case.

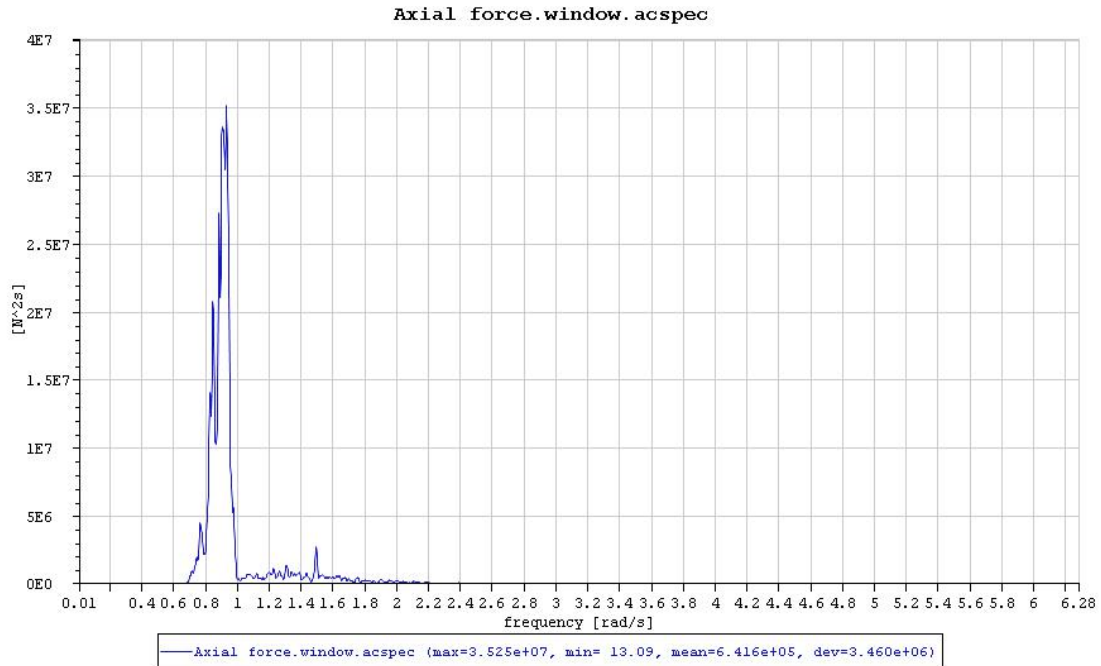


Figure 6-2. Tension power spectrum on Hs=1m, Tp=5s.

6.3. Dynamic analysis

Based on the static analysis, the wave load and vessel motion are applied to the riser system. The dynamic response analysis of the riser system focus on four variables. These are the vertical displacement of the node along the riser, the axial tension, the bending moment of the upper part of the riser and the associated stress. Because there is selected 113 kinds of sea states in the whole analysis, as an example, considering the most probable sea state of Hs=2m, Tp=8s.

6.3.1. Vertical Displacement

Due to the heave motion of the vessel, it will lead to large vertical displacement of the node along the riser. From the Figure6-3, it can be seen that the end node has the maximum vertical displacement. Therefore, in the next step, it just needs to be analyze the maximum vertical displacement of the end node. That maximum vertical displacement fluctuates around the initial static equilibrium position, which can be found in Figure6-4. The absolute values of the maximum vertical displacement of the end node of the selected sea states are shown in Table6-1.

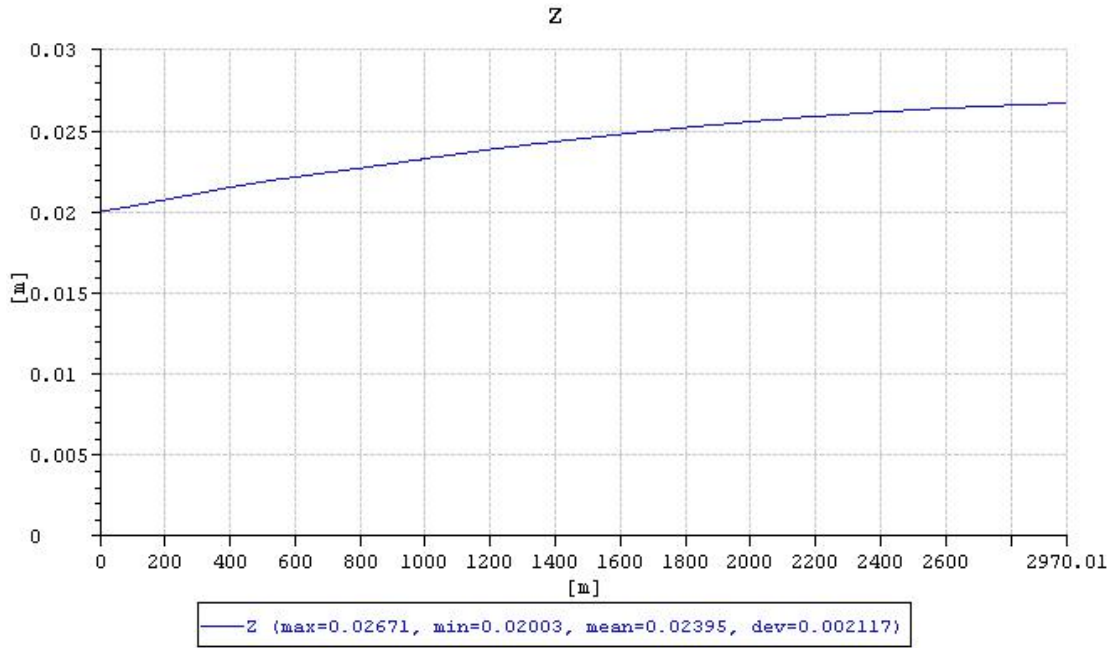


Figure 6-3. The displacement standard deviation of the riser on $H_s=2\text{m}$, $T_p=8\text{s}$.

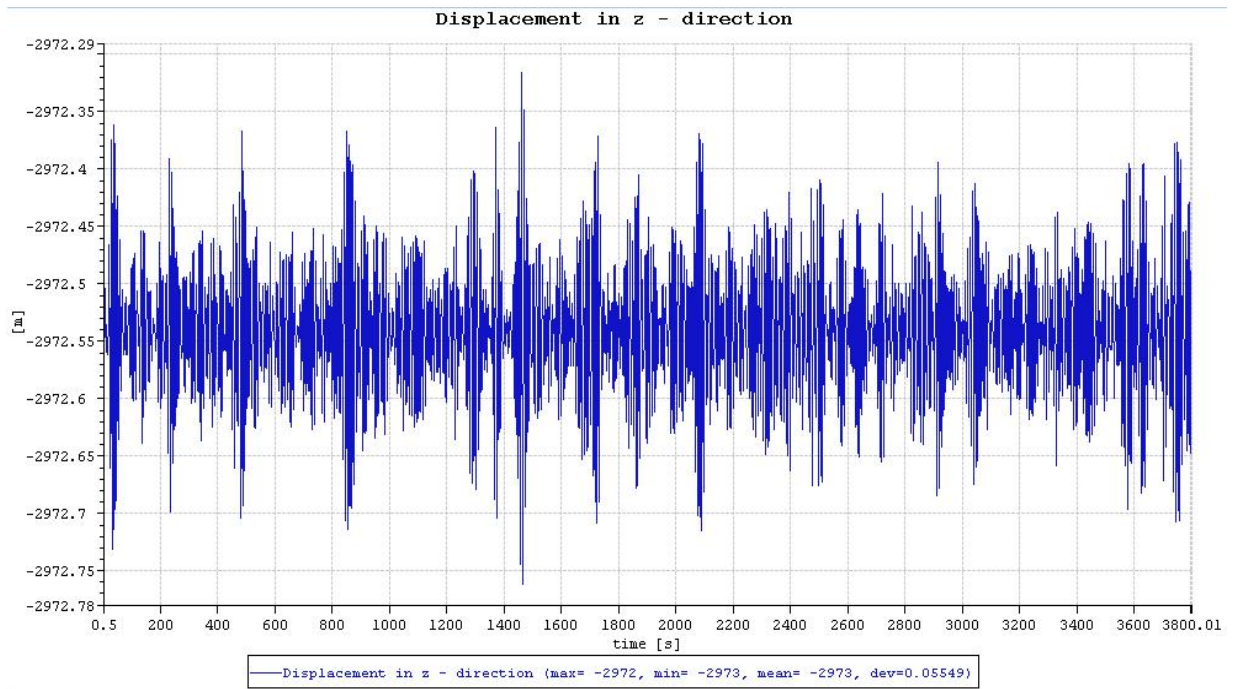


Figure 6-4. The displacement of the final node of the riser on $H_s=2\text{m}$, $T_p=8\text{s}$.

Table 6-1. The absolute value of maximum vertical displacement (m) of the end node of selected sea states.

<div style="display: inline-block; transform: rotate(-45deg);">Tp</div> <div style="display: inline-block; transform: rotate(-45deg);">Hs</div>	5	6	7	8	9	10	11	12	13	14	15	16	17	18	19
1	0,005	0,021	0,055	0,113	0,179	0,239	0,292	0,345	0,385	0,410	0,418	0,421	0,440	0,510	0,469
2	0,007	0,038	0,109	0,225	0,358	0,479	0,586	0,693	0,774	0,826	0,841	0,850	0,881	1,021	0,940
3	0,011	0,049	0,146	0,336	0,538	0,719	0,881	1,041	1,166	1,246	1,267	1,284	1,322	1,532	1,412
4		0,065	0,178	0,439	0,745	0,959	1,179	1,392	1,559	1,669	1,696	1,720	1,764	2,043	1,885
5			0,223	0,533	0,958	1,281	1,493	1,746	1,954	2,096	2,125	2,160	2,121	2,556	2,359
6				0,640	1,163	1,604	1,893	2,126	2,349	2,525	2,555	2,601	2,650	3,069	
7					1,359	1,922	2,296	2,589	2,766	2,956	2,986	3,043	3,094	3,582	
8						2,221	2,694	3,052	3,253	3,399	3,417	3,486	3,539		
9							3,082	3,510	3,752	3,906	3,847	3,928	3,985		
10								3,957	4,250	4,412	4,319	4,370			

6.3.2. Axial tension

Comparing the quasi-static effective tension curve and the force envelope curve for $H_s=10m$, $T_p=16s$, it can be found that the tension along the riser is increasing. Moreover, the maximum axial tension along the riser is at the top of the riser. Therefore, the element 1 of the riser is chosen to analyze the maximum axial tension in the dynamic analysis.

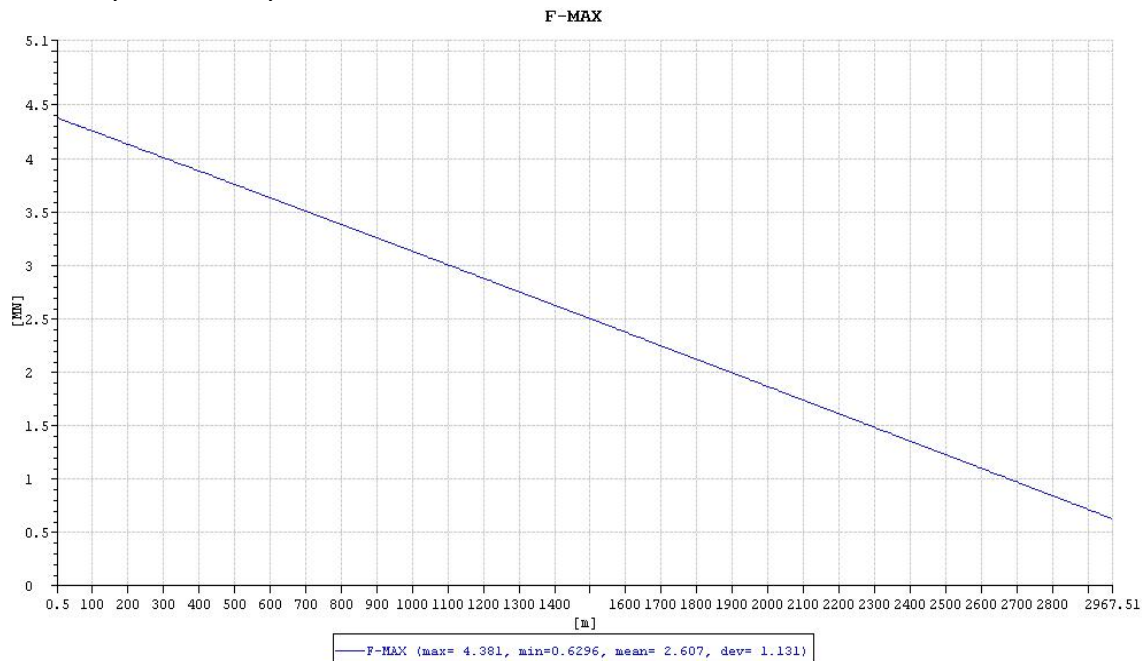


Figure 6-5. The force envelope curve of the riser on $H_s=2m$, $T_p=8s$.

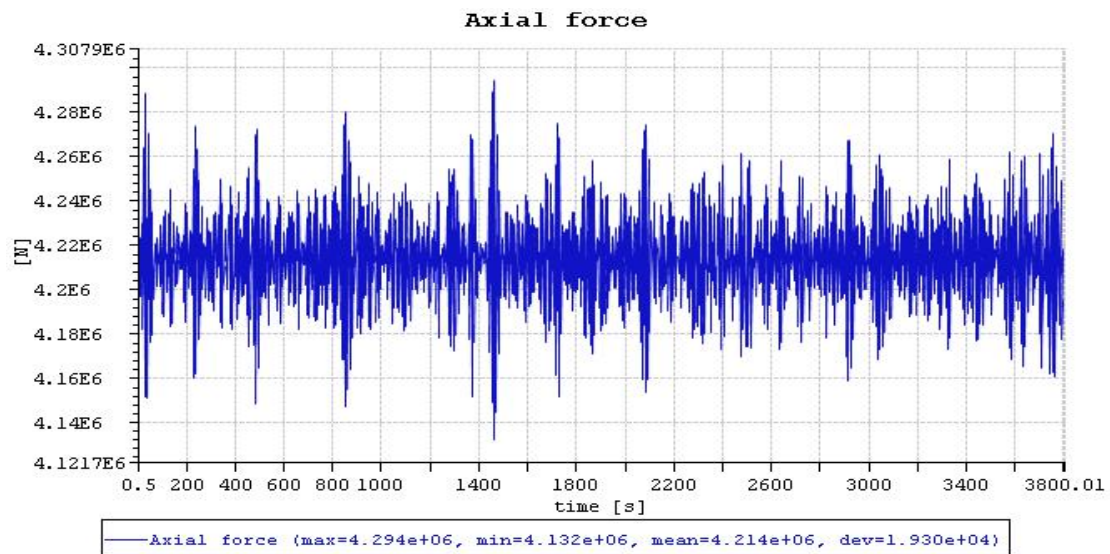


Figure 6-6. The axial tension of element 1 of the riser on $H_s=2\text{m}$, $T_p=8\text{s}$.

The axial tension of element 1 fluctuates around the initial static equilibrium position, which is shown in Figure 6-6. The maximum axial tension of the riser under the selected sea states are listed in the Table 6-2. It is noticed that there is small axial resonance comparing with the quasi-static effective tension.

Table 6-2. The maximum axial tension(MN) of the element 1 of selected sea states.

T_p H_s	5	6	7	8	9	10	11	12	13	14	15	16	17	18	19
1	4.217	4.224	4.237	4.254	4.270	4.284	4.294	4.300	4.296	4.297	4.300	4.295	4.292	4.291	4.287
2	4.219	4.232	4.259	4.294	4.326	4.354	4.377	4.392	4.385	4.387	4.394	4.382	4.373	4.370	4.361
3	4.221	4.239	4.276	4.335	4.383	4.427	4.463	4.488	4.478	4.484	4.494	4.475	4.457	4.451	4.436
4		4.247	4.296	4.375	4.454	4.503	4.551	4.587	4.574	4.586	4.597	4.571	4.545	4.533	4.512
5			4.317	4.413	4.533	4.611	4.646	4.690	4.672	4.693	4.703	4.670	4.634	4.617	4.590
6				4.452	4.611	4.724	4.770	4.802	4.775	4.803	4.811	4.771	4.726	4.703	
7					4.683	4.839	4.897	4.940	4.886	4.915	4.919	4.873	4.820	4.790	
8						4.949	5.034	5.080	5.019	5.032	5.034	4.977	4.915		
9							5.173	5.221	5.153	5.160	5.152	5.082	5.013		
10								5.366	5.290	5.288	5.271	5.187			

6.3.3. Bending moment

The bending moment is discussed under the local riser coordinate system. Resulting from the pin joint applied at the top of the riser, the bending moment at the top and the bottom of the riser is zero. This is visualised in Figure6-7 and 6-8. Figure6-8 is a partial enlarged view of Figure6-7.

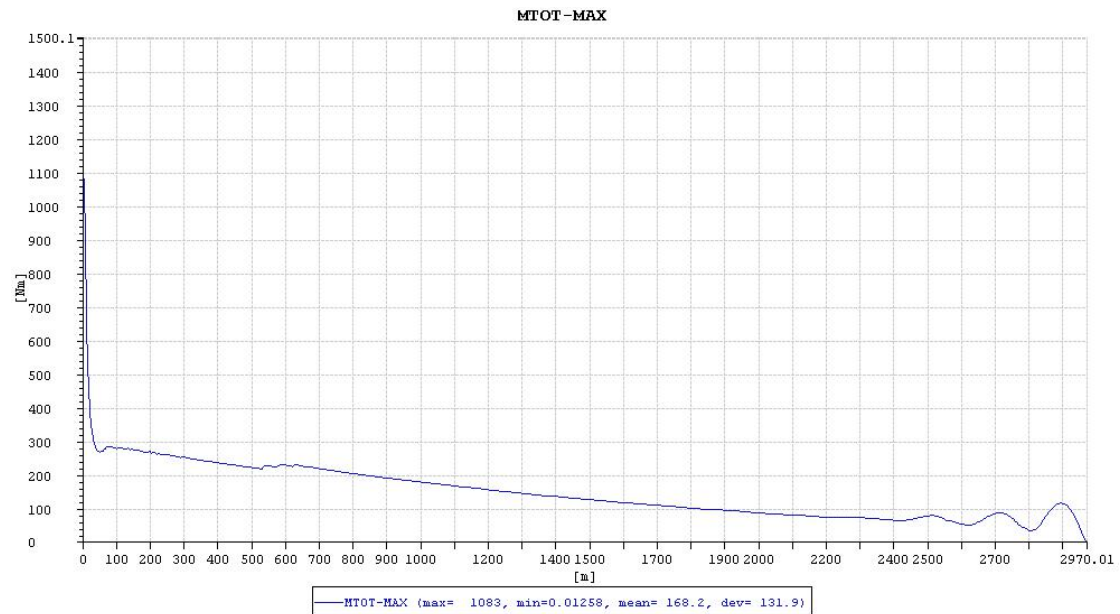


Figure 6-7. The total bending moment along the riser on $H_s=2\text{m}$, $T_p=8\text{s}$.

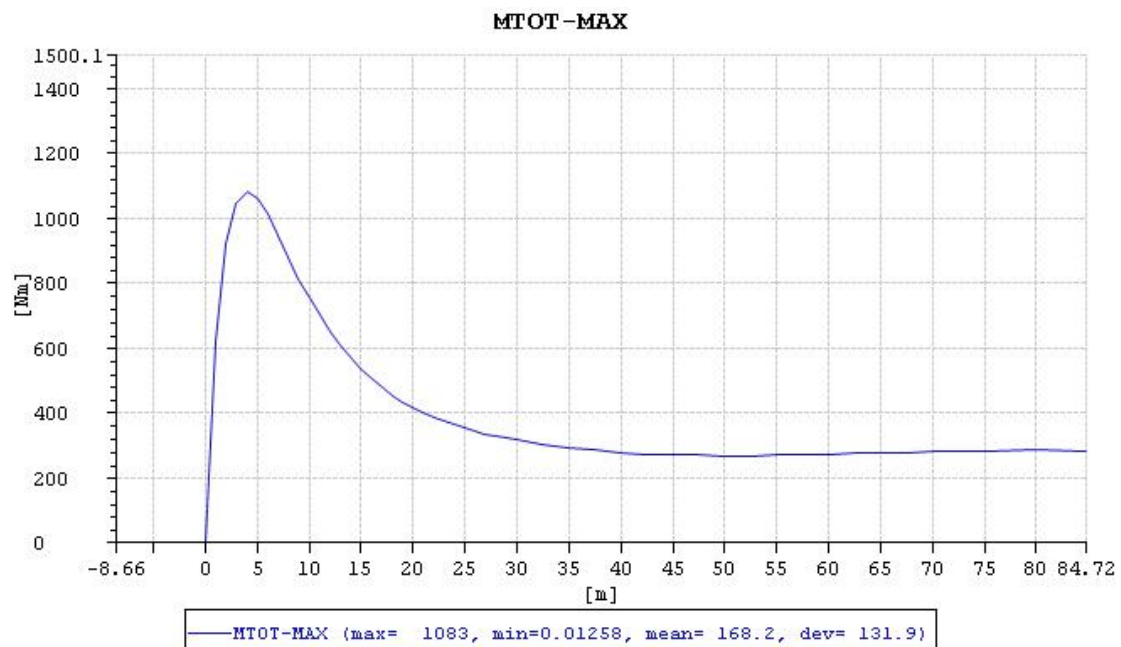


Figure 6-8. The partial enlarged view of total bending moment along the riser on $H_s=2\text{m}$, $T_p=8\text{s}$.

From Figure 6-9 and Figure 6-10 , it can be seen that the absolute value of the bending moment in y-direction is much larger than in z-direction. It can be known that the wave loading comes from the y-direction of the riser. The maximum bending moment discussed in this thesis is the maximum total bending moment which is combined by the maximum bending moment in y and z direction.

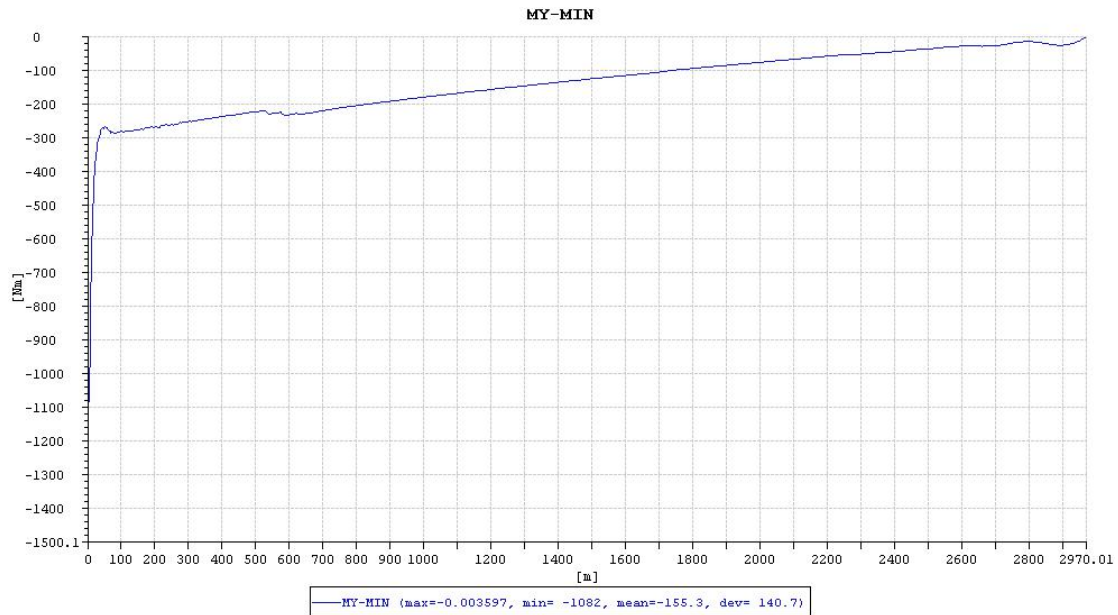


Figure 6-9. The y-direction bending moment along the riser on $H_s=2m$, $T_p=8s$.

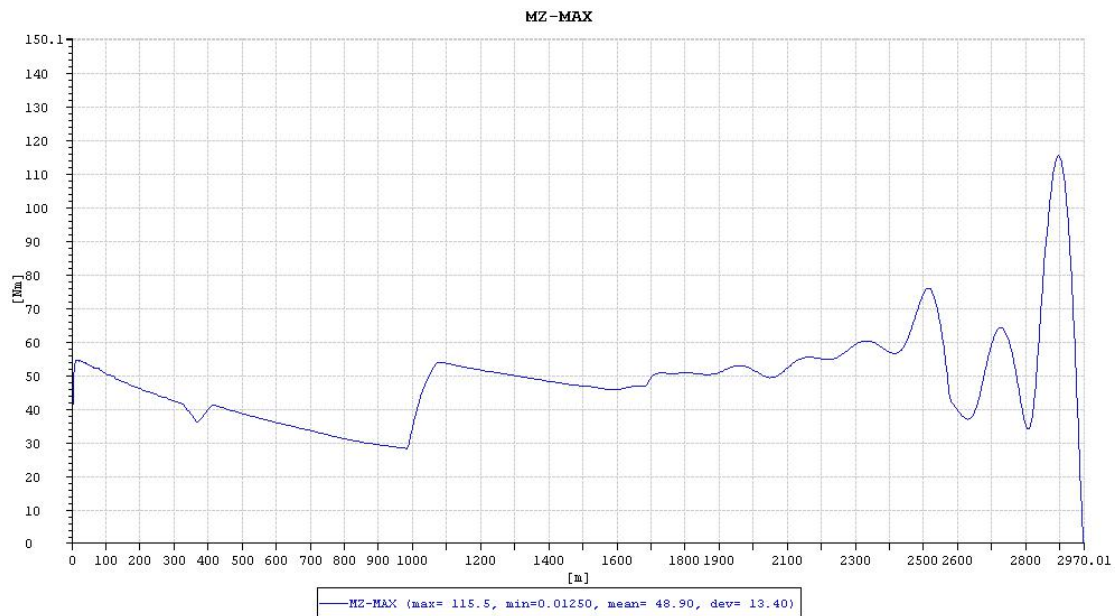


Figure 6-10. The z-direction bending moment along the riser on $H_s=2m$, $T_p=8s$.

The elements where the maximum bending moments are located of selected sea states are listed in the the Table6-3. It can be found that the maximum bending moments along the riser are within the top ten meter. They occur at the top because they are related to local wave action. From Table6-4, it can be seen that the value of maximum bending moment are extremely small. The reason for this phenomenon is that the large tension gives large stiffness that results in the small bending moment.

Table 6-3. The location of the total maximum bending moment along the riser of selected sea states.

T_p H_s	5	6	7	8	9	10	11	12	13	14	15	16	17	18	19
1	4	3	4	4	4	5	5	5	6	6	6	6	6	6	7
2	3	3	4	4	4	4	4	4	5	5	6	6	6	6	6
3	3	3	3	4	4	4	4	4	6	4	5	5	6	6	6
4		3	3	4	4	4	4	4	5	4	5	5	5	5	6
5			3	4	4	4	4	4	4	4	5	5	5	5	5
6				3	4	4	3	4	5	4	5	5	5	5	
7					4	4	3	4	4	4	5	5	5	5	
8						4	2	4	4	4	4	4	5		
9							3	4	4	4	4	4	5		
10								5	5	4	5	5			

Table 6-4. The total maximum bending moment(Nm) of the riser of selected sea states.

T_p H_s	5	6	7	8	9	10	11	12	13	14	15	16	17	18	19
1	915	913	958	631	787	638	436	346	336	471	459	404	355	318	285
2	2096	1717	1859	1083	1553	1123	662	487	451	788	714	591	487	411	342
3	3593	2546	2463	1459	2528	1716	896	706	640	1182	993	796	622	506	402
4		3790	3042	1708	3312	2395	1139	1002	913	1648	1291	1019	765	603	462
5			4081	1946	3994	3295	1391	1304	1260	2184	1633	1255	913	699	523
6				2421	4665	4385	1765	1594	1689	2789	2014	1511	1064	795	
7					5756	5637	2440	1840	2221	3477	2427	1782	1223	890	
8						6995	3227	2077	2927	4209	2878	2070	1388		
9							4108	2302	3715	4808	3368	2374	1558		
10								2515	4581	5411	3603	2697			

6.3.4. Riser stress

In this case, the riser stress is the resultant stress, which is formed by the axial tension stress and the bending moment stress. It can be found from the following formula:

$$\sigma_R = \sigma_T + \sigma_M \quad (6-2)$$

$$\sigma_R = \frac{T}{A} + \frac{M_y * r}{I} + \frac{M_z * r}{I} \quad (6-3)$$

Where:

σ_R is the resultant stress;

σ_T is the axial tension stress;

σ_M is the bending moment stress;

T is the axial tension;

M_y is the bending moment in y direction;

M_z is the bending moment in z direction;

I is the moment of inertia,

r is the radius to point in cross-section (outer or inner radius).

The riser stress can be obtained by the post processor package of SIMA. Moreover, to find which point has the greatest stress along the outer wall of the riser, it takes eight equal diversion points along the outer wall of the riser. Which can be shown in Figure6-11.

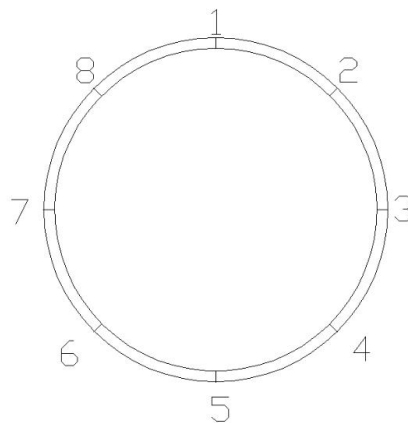


Figure 6-11. The schematic diagram of eight equal diversion points along the outer wall of the riser.

Due to the in plane top loading of the riser applied in this study, the maximum stress of the riser is in the horizontal direction. In this pinned connection case, the point of

maximum stress along the outer wall of the riser is the point 3. The fluctuation of the resultant stress in the time domain of the point 3 can be seen in Figure6-12. The maximum stress of the riser in various sea states are listed in Table6-5.

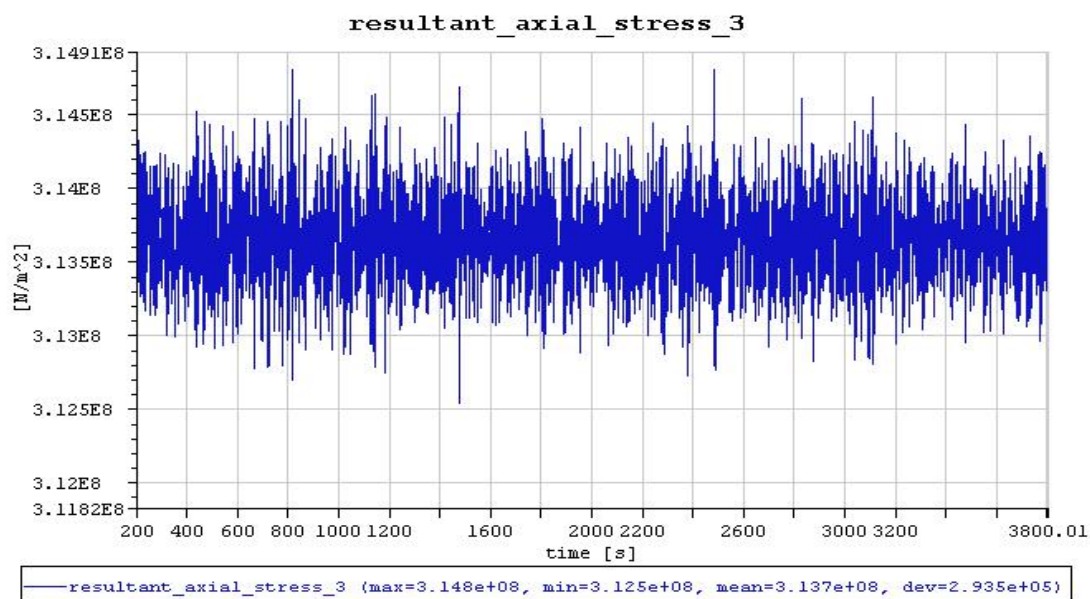


Figure 6-12. The resultant stress in the time domain of the point 3 on Hs=1m, Tp=5s.

Table 6-5. The maximum stress (Mpa) of selected sea states.

T_p H_s	5	6	7	8	9	10	11	12	13	14	15	16	17	18	19
1	315	315	315	316	318	319	320	320	320	320	320	320	319	319	318
2	317	317	317	320	322	324	326	327	327	326	327	326	325	325	324
3	319	320	318	323	327	329	332	334	334	333	334	333	331	331	329
4		324	321	325	332	335	339	341	341	341	342	340	338	337	335
5			325	328	338	343	346	349	348	349	350	348	344	344	341
6				330	343	351	355	357	356	356	358	355	351	350	
7					348	359	365	366	364	364	366	363	358	357	
8						366	374	376	373	372	374	370	365		
9							384	387	383	381	383	378	373		
10								398	393	390	391	385			

6.4. Fatigue analysis

The fatigue analysis is based on the method described in Section 4. The probability of the occurrence of the selected sea states is listed in Table6-6.

Table 6-6. The probability of the occurrence of selected sea states.

T_p H_s	5	6	7	8	9	10	11	12	13	14	15	16	17	18	19
1	0.01071	0.01583	0.01649	0.01374	0.00991	0.00649	0.00399	0.00234	0.00133	0.00075	0.00041	0.00022	0.00012	0.00007	0.00004
2	0.01244	0.03253	0.05153	0.05867	0.05332	0.04140	0.02890	0.01838	0.01108	0.00640	0.00358	0.00196	0.00106	0.00057	0.00030
3	0.00147	0.00839	0.02316	0.03932	0.04750	0.04497	0.03563	0.02474	0.01557	0.00909	0.00502	0.00265	0.00136	0.00068	0.00033
4		0.00086	0.00485	0.01384	0.02428	0.02987	0.02822	0.02183	0.01450	0.00857	0.00462	0.00233	0.00111	0.00050	0.00022
5			0.00058	0.00318	0.00906	0.01578	0.01896	0.01712	0.01239	0.00755	0.00402	0.00193	0.00085	0.00035	0.00013
6				0.00039	0.00209	0.00576	0.00959	0.01079	0.00893	0.00580	0.00312	0.00143	0.00059	0.00021	
7					0.00027	0.00137	0.00350	0.00533	0.00538	0.00391	0.00219	0.00099	0.00037	0.00012	
8						0.00020	0.00089	0.00199	0.00263	0.00228	0.00139	0.00065	0.00023		
9							0.00015	0.00054	0.00102	0.00112	0.00079	0.00039	0.00014		
10								0.00011	0.00030	0.00045	0.00039	0.00022			

In addition, E curve were selected as the S-N curve by the DNV-OS-C203 (2011), which was shown in Section 3. The results of fatigue analysis is presented as the fatigue life of the riser system. The fatigue life of riser with pinned topside connection by different riser stress are shown in the Figure6-13, 6-14 and 6-15.

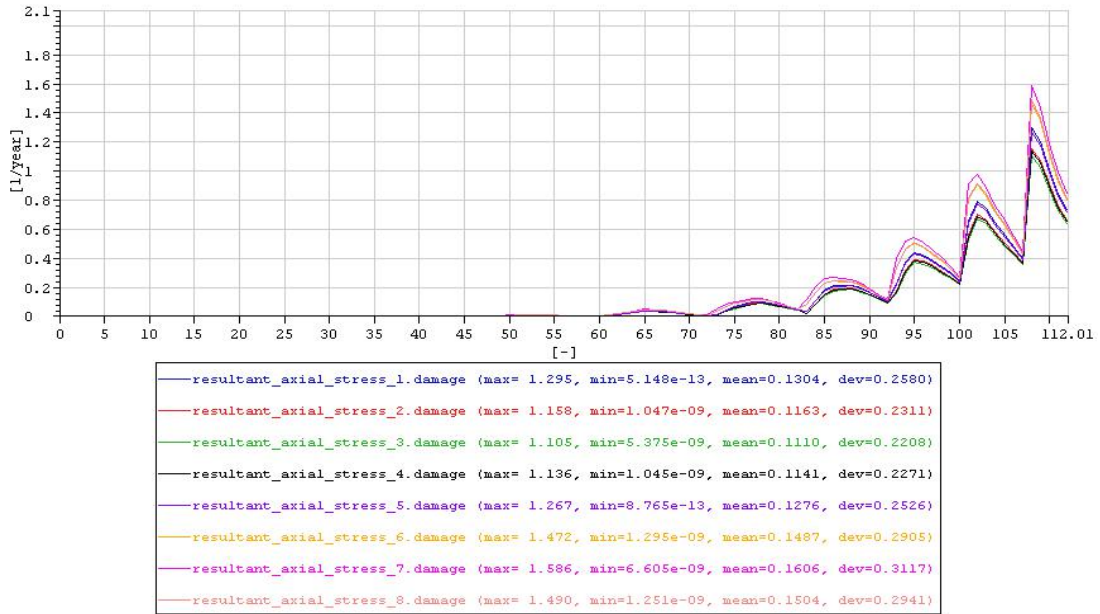


Figure 6-13. The fatigue life of riser with pinned topside connection by resultant stress.

The maximum fatigue life of riser with pinned topside connection by resultant stress is 1/1.6 year. Then when including the safety fact DFF=10, the fatigue life is 1/16 year, which is around 3 weeks.

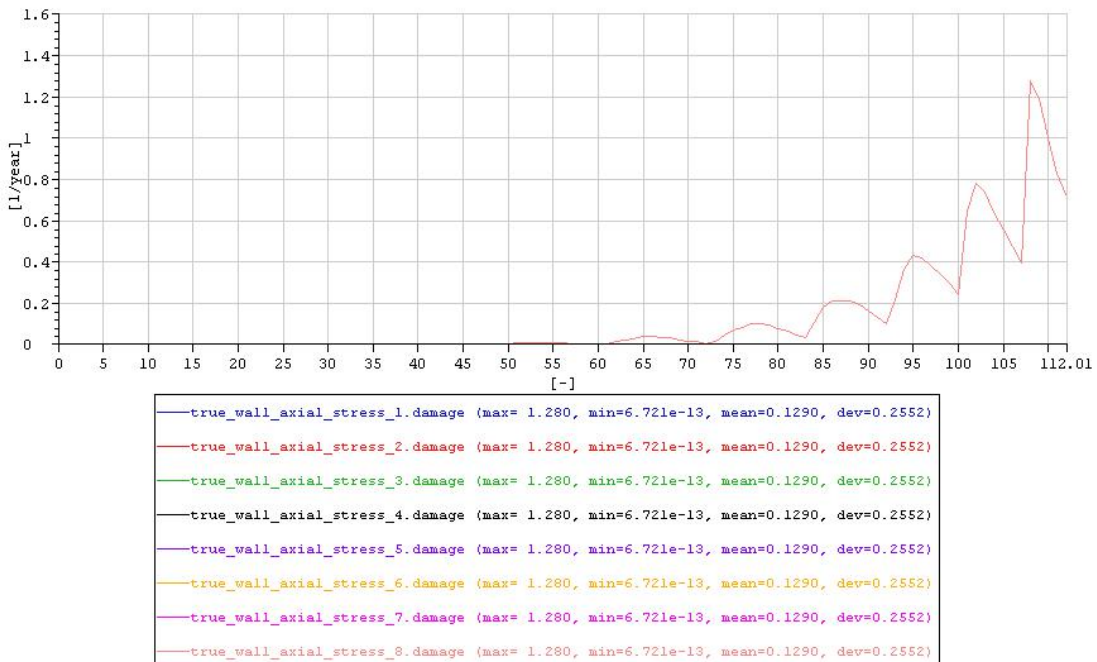


Figure 6-14. The fatigue life of riser with pinned topside connection by only axial tension stress.

If just the axial tension stress is considered in the fatigue analysis, the fatigue life is 1/13 year, around one month. This means that the tension dynamics is important.

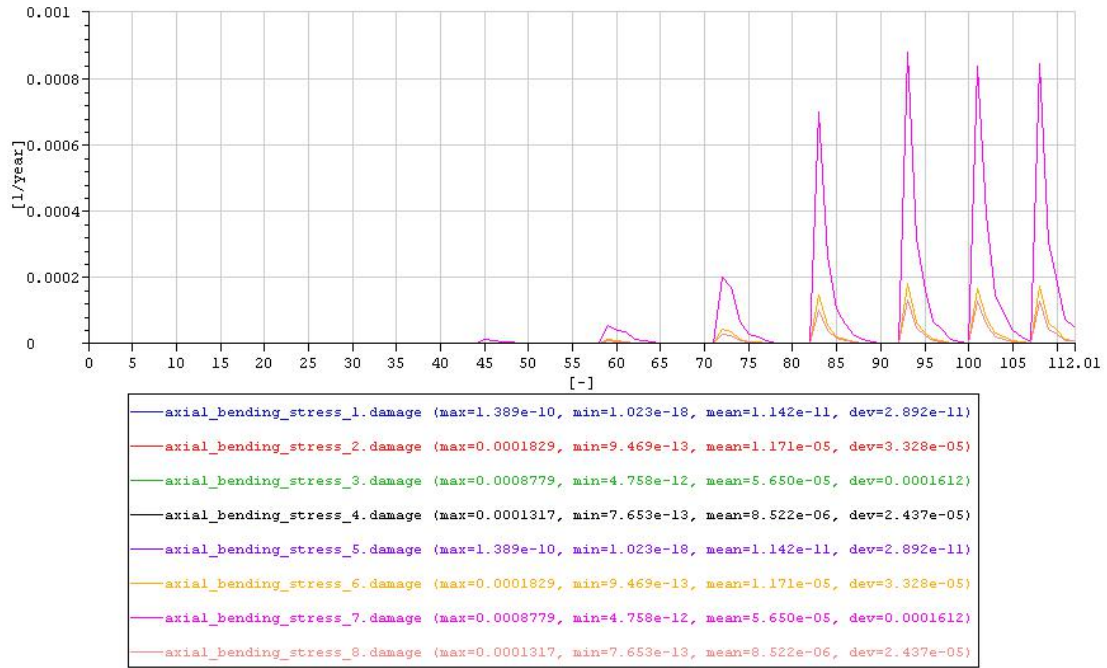


Figure . The fatigue life of riser with pinned topside connection by only bending moment stress.

If only the bending moment stress is considered in the fatigue analysis, the fatigue life will be around 113 year.

7. Fixed topside connection analysis results

This section gives results for the fixed topside connection case, which means that the top of the riser is rotationally fixed to the vessel. This section has similar response as described in Section 6 with respect to effective tension, vertical displacement and axial tension. However, the top local bending behaviour will be different.

7.1. Quasi-static analysis

7.1.1. Effective tension

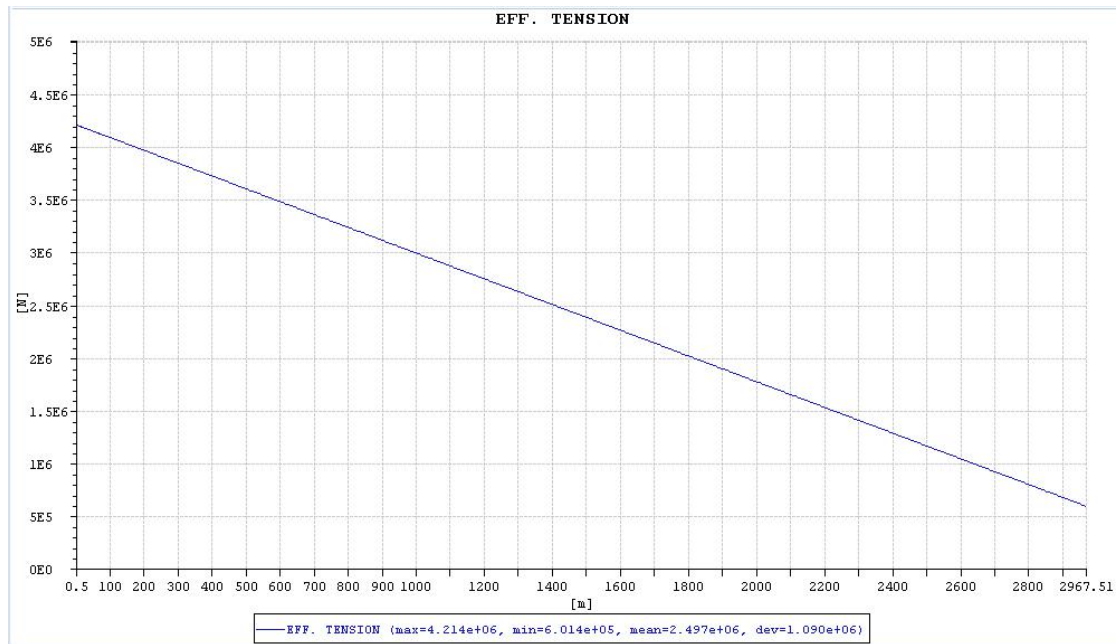


Figure 7-1. The quasi-static effective tension of the riser.

7.2. Dynamic analysis

7.2.1. Vertical Displacement

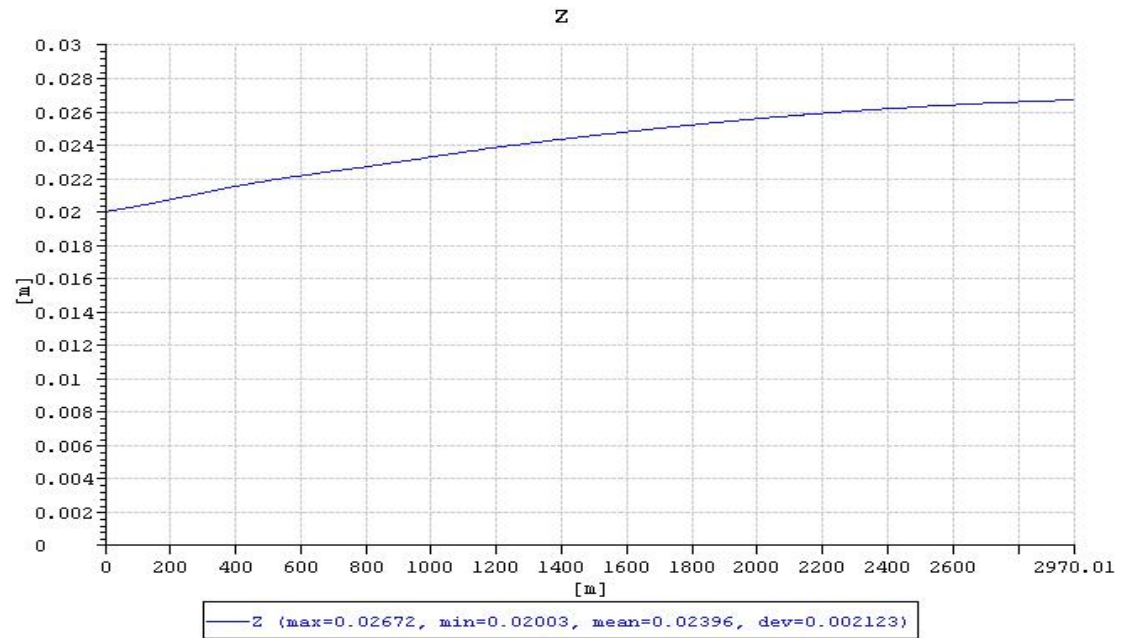


Figure 7-2. The displacement standard deviation of the riser on $H_s=2\text{m}$, $T_p=8\text{s}$.

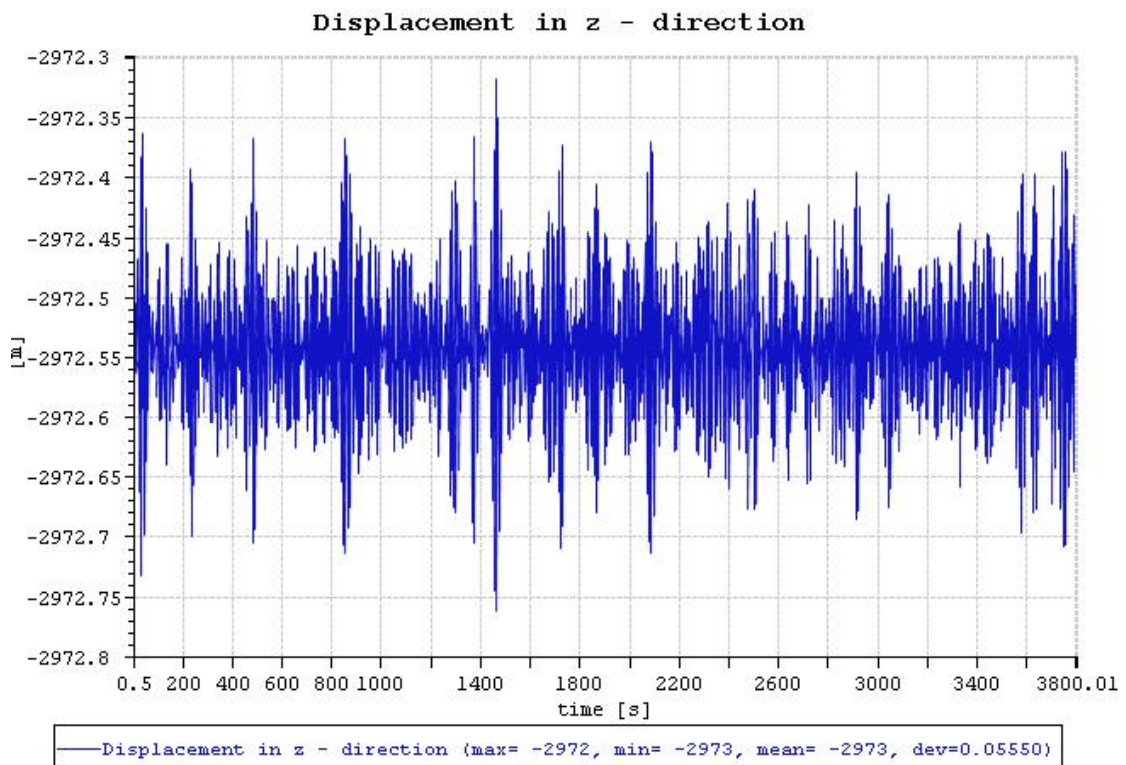


Figure 7-3. The displacement of the final node of the riser on $H_s=2\text{m}$, $T_p=8\text{s}$.

Table 7-1. The absolute value of maximum vertical displacement (m) of the end node of selected sea states.

Tp Hs	5	6	7	8	9	10	11	12	13	14	15	16	17	18	19
1	0,005	0,021	0,055	0,113	0,179	0,239	0,292	0,345	0,385	0,410	0,418	0,421	0,440	0,510	0,469
2	0,007	0,038	0,110	0,225	0,358	0,479	0,586	0,693	0,774	0,826	0,841	0,850	0,881	1,021	0,940
3	0,011	0,049	0,146	0,336	0,538	0,719	0,881	1,041	1,167	1,246	1,267	1,284	1,322	1,532	1,413
4		0,066	0,179	0,439	0,745	0,959	1,178	1,392	1,560	1,670	1,695	1,721	1,764	2,043	1,885
5			0,223	0,534	0,959	1,280	1,492	1,745	1,955	2,097	2,124	2,161	2,123	2,555	2,360
6				0,640	1,164	1,604	1,892	2,125	2,351	2,265	2,554	2,604	2,649	3,068	
7					1,360	1,921	2,294	2,587	2,769	2,958	2,984	3,046	3,093	3,581	
8						2,219	2,691	3,050	3,257	3,402	3,414	3,490	3,538		
9							3,079	3,507	3,755	3,910	3,844	3,932	3,983		
10								3,954	4,254	4,417	4,316	4,375			

7.2.2. Axial tension

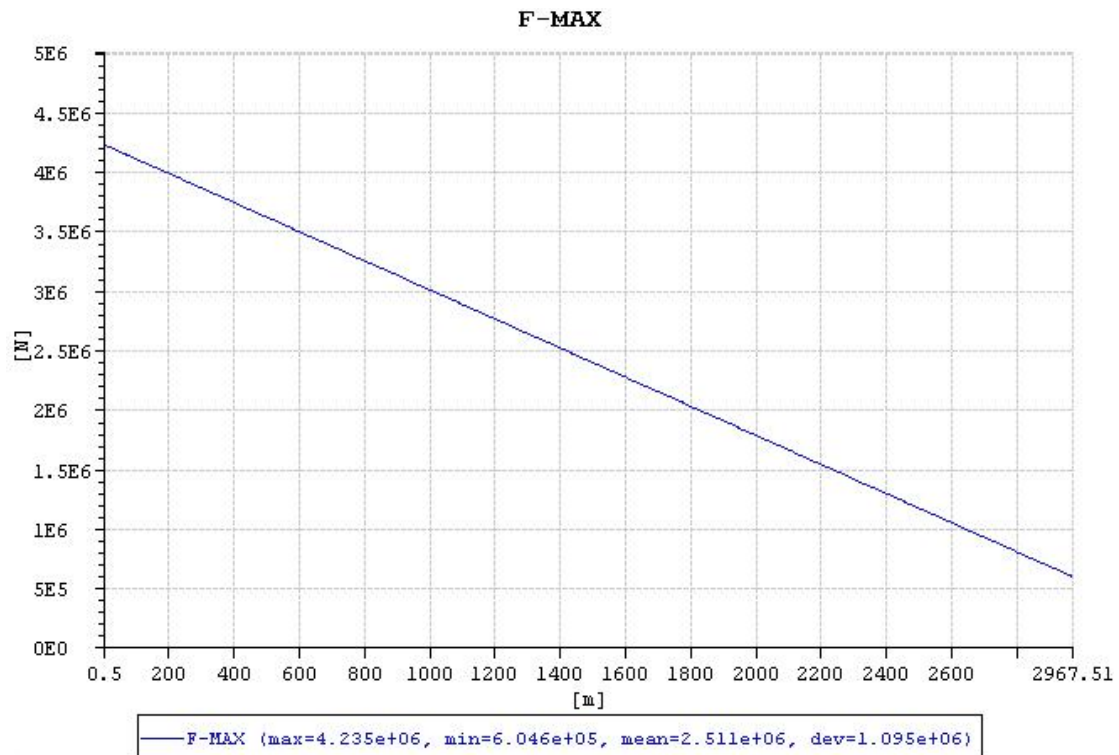


Figure 7-4. The force envelope curve of the riser on Hs=2m, Tp=8s.

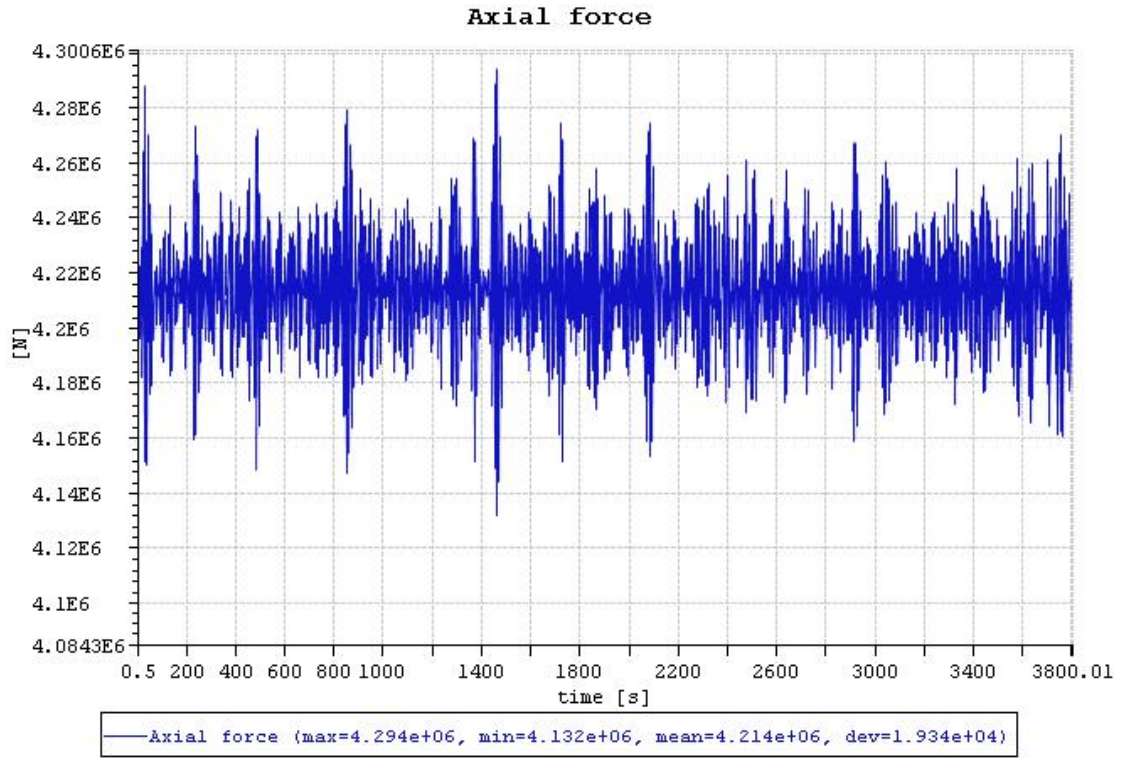


Figure 7-5. The axial tension of element 1 of the riser on Hs=2m, Tp=8s.

Table 7-2. The maximum axial tension(MN) of the element 1 of selected sea states.

T_p H_s	5	6	7	8	9	10	11	12	13	14	15	16	17	18	19
1	4.217	4.224	4.237	4.254	4.270	4.284	4.294	4.300	4.296	4.297	4.300	4.294	4.292	4.291	4.287
2	4.219	4.232	4.259	4.294	4.326	4.354	4.377	4.392	4.385	4.387	4.394	4.382	4.373	4.370	4.361
3	4.221	4.238	4.276	4.335	4.383	4.427	4.463	4.488	4.478	4.484	4.494	4.475	4.457	4.451	4.436
4		4.247	4.296	4.375	4.454	4.503	4.551	4.588	4.574	4.586	4.598	4.571	4.545	4.533	4.512
5			4.316	4.412	4.533	4.611	4.646	4.690	4.672	4.694	4.703	4.670	4.634	4.617	4.590
6				4.452	4.611	4.724	4.770	4.802	4.775	4.804	4.811	4.771	4.726	4.703	
7					4.684	4.839	4.897	4.940	4.887	4.916	4.919	4.873	4.820	4.790	
8						4.950	5.034	5.081	5.020	5.032	5.035	4.977	4.916		
9							5.174	5.222	5.154	5.162	5.153	5.082	5.013		
10								5.367	5.291	5.289	5.273	5.188			

7.2.3. Bending moment

The bending moment is discussed under the local riser coordinate system. Resulting from the top of the riser is fixed to the vessel, the maximum bending moment is located at the top of the riser, but the end of the riser is zero. The above information can be seen in Figure 7-6 and 7-7. Figure 7-7 is a partial enlarged view of Figure 7-6.

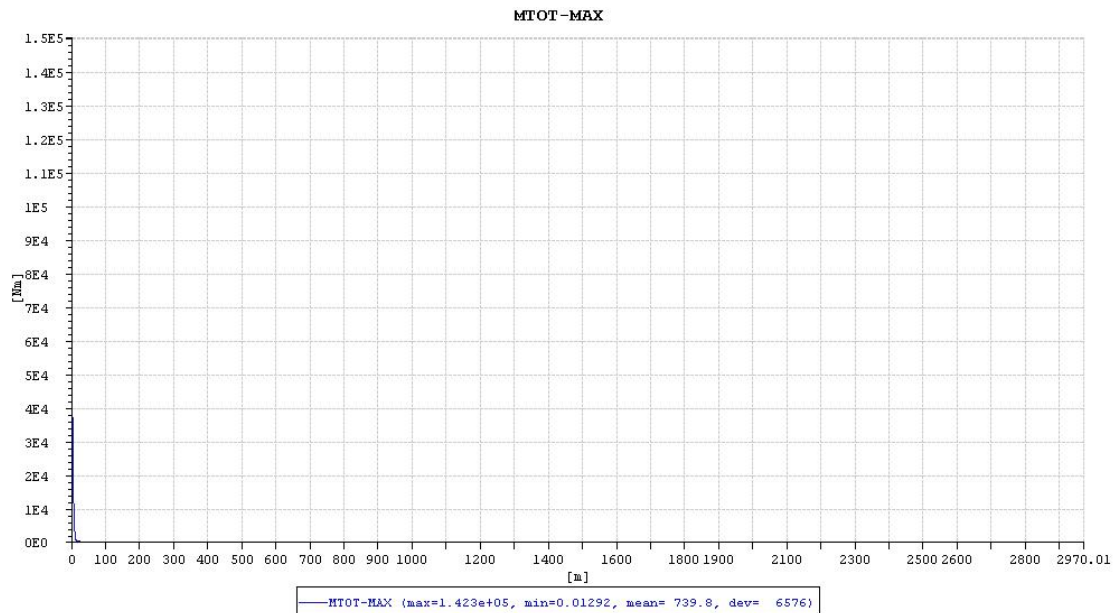


Figure 7-6. The total bending moment along the riser on $H_s=2m$, $T_p=8s$.

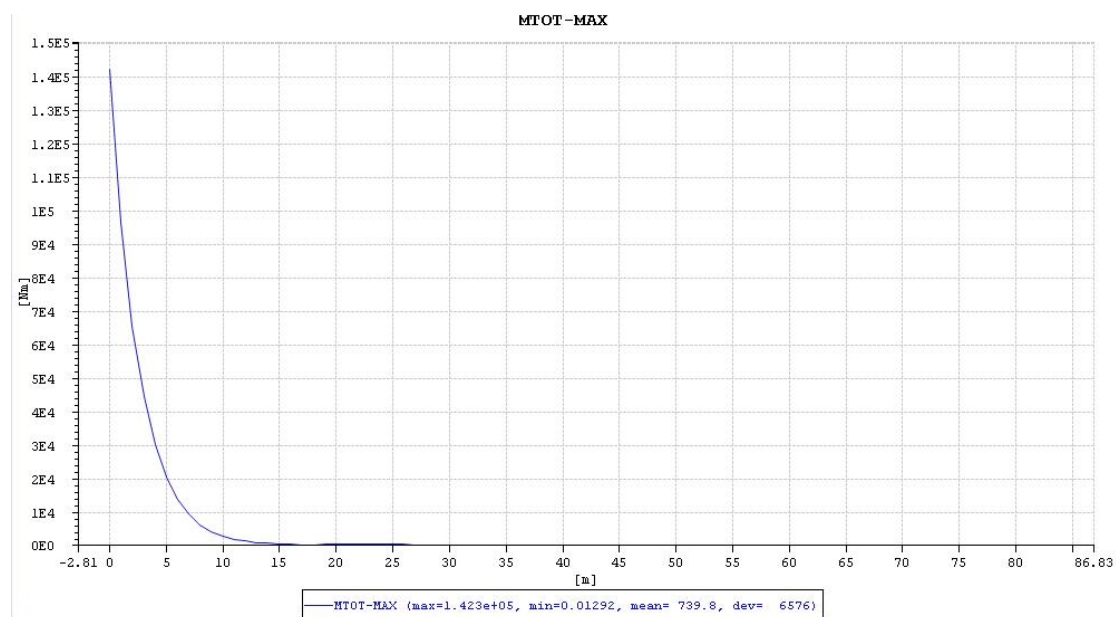


Figure 7-7. The partial enlarged view of total bending moment along the riser on $H_s=2m$, $T_p=8s$.

In this section the maximum bending moment is also the total bending moment. From the Figure7-6 and 7-7, it can be known that the maximum bending moment is at the element 1 of the riser. Therefore, the maximum bending moment of riser of the selected sea states are listed in Table7-3.

Table 7-3. The total maximum bending moment (KNm) of riser of selected sea states.

T_p H_s	5	6	7	8	9	10	11	12	13	14	15	16	17	18	19
1	134	135	141	137	147	145	146	148	146	151	151	150	149	149	149
2	139	139	151	142	163	159	161	165	161	172	171	169	168	167	166
3	145	145	156	147	180	174	176	182	177	194	192	188	187	186	185
4		150	160	153	196	190	191	199	193	218	213	209	206	205	203
5			169	160	210	225	210	217	209	242	236	230	227	225	223
6				166	224	266	247	240	226	267	260	253	248	246	
7					241	310	289	280	245	294	285	275	270	268	
8						352	333	322	290	325	310	298	292		
9							378	367	340	381	335	321	313		
10								413	393	440	376	344			

7.2.4. Riser stress

The riser stress is also represented by the resultant stress in the fixed connection case. Moreover, the point of maximum stress along the outer wall of the riser is point 7, which can be found in Figure6-11. The fluctuation of the resultant stress in the time domain of the point 7 can be seen in Figure7-8. The maximum stress of the riser in various sea states are listed in Table7-4.

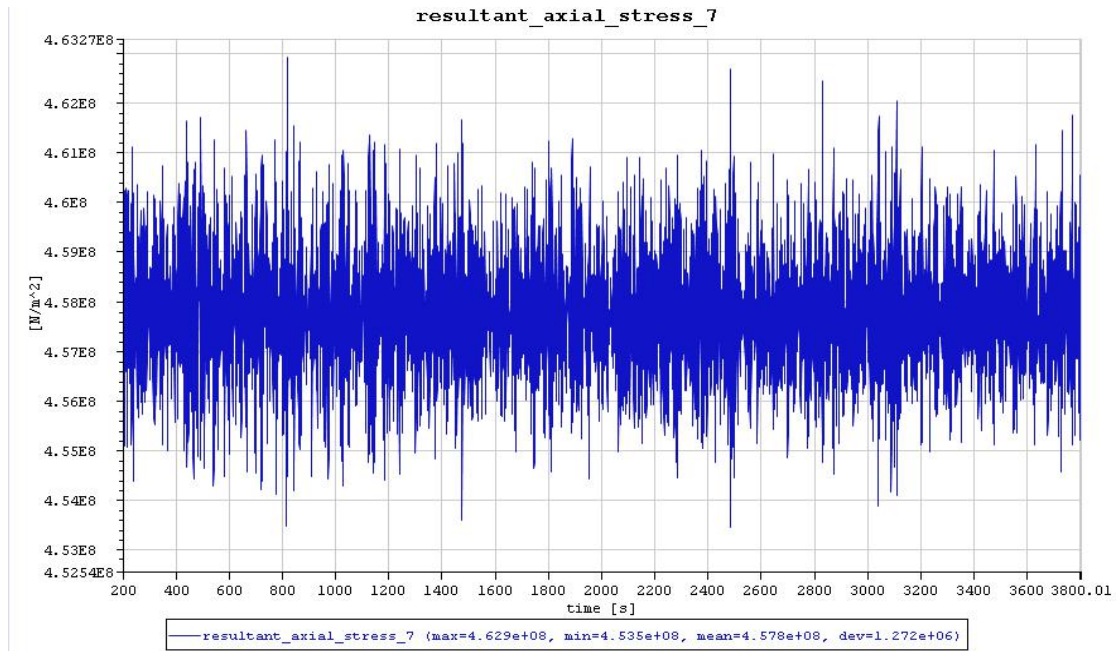


Figure 7-8. The resultant stress in the time domain of the point 3 on Hs=1m, Tp=5s.

Table 7-4. The maximum stress (Mpa) of the riser of selected sea states.

Tp Hs	5	6	7	8	9	10	11	12	13	14	15	16	17	18	19
1	463	467	481	495	513	530	538	551	556	558	561	565	566	551	556
2	469	477	505	534	570	603	620	647	657	662	670	676	678	649	657
3	478	486	522	573	629	678	705	745	761	770	783	793	795	752	761
4		501	539	613	705	755	792	847	869	881	902	915	917	860	868
5			562	651	789	866	888	952	980	996	1025	1042	1043	971	978
6				693	875	982	1018	1068	1094	1116	1150	1171	1173	1083	
7					957	1101	1151	1214	1219	1239	1277	1304	1305	1197	
8						1216	1287	1363	1368	1369	1406	1438	1439		
9							1422	1514	1522	1519	1538	1575	1576		
10								1665	1679	1674	1682	1715			

7.3. Fatigue analysis

The same procedure as described in the Section 6.4 was repeated, and the results are shown in Figure7-9,7-10and 7-11.



Figure 7-9. The fatigue life of riser with fixed topside connection by resultant stress.

The maximum fatigue life of riser with fixed topside connection by resultant stress is 1/3806 year. Then when including the safety fact DFF=10, the fatigue life is 1/38060 year, which is around 15 minutes.

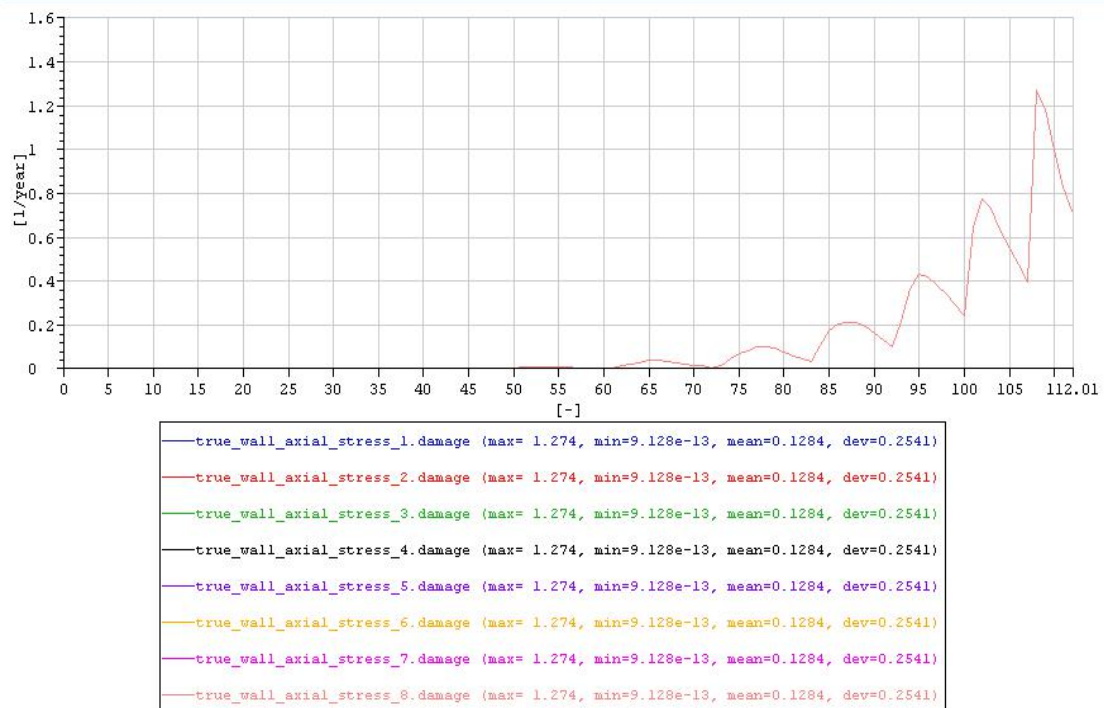


Figure 7-10. The fatigue life of riser with fixed topside connection by only axial tension stress.

If just the axial tension stress is considered in the fatigue analysis, the fatigue life is 1/13 year, around one month.

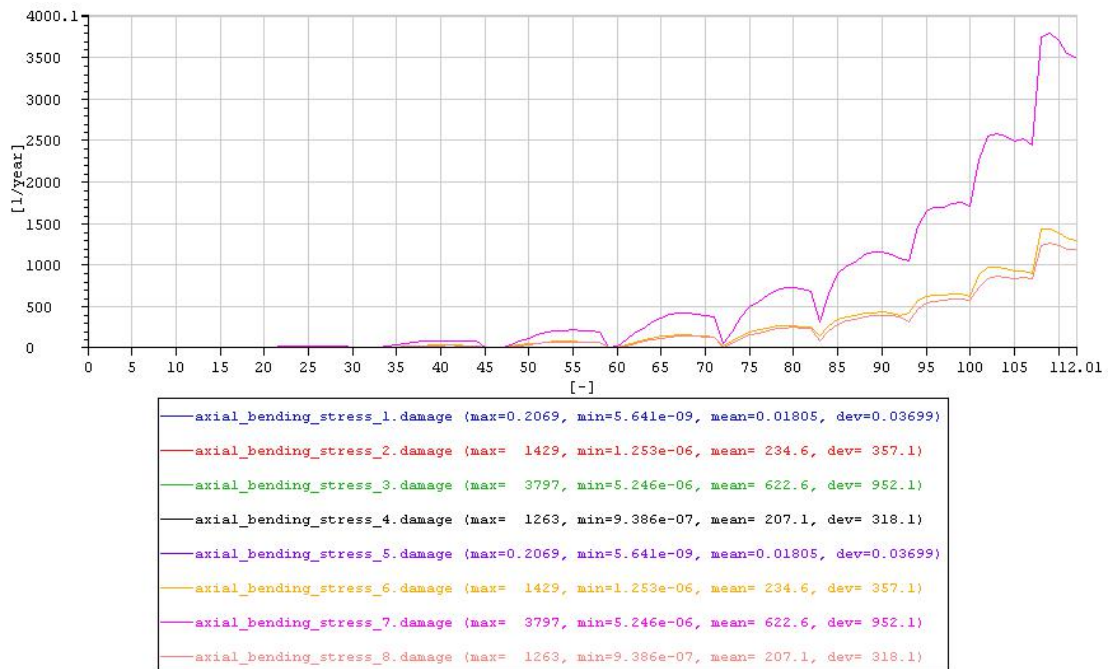


Figure 7-11. The fatigue life of riser with fixed topside connection by only bending moment stress.

If only the bending moment stress is considered in the fatigue analysis, the fatigue life is 1/37970 year, around 15 minutes.

8. Comparison and analysis

The results for two topside connection cases have been presented in the Chapter 6 and Chapter 7. This chapter will compare the results, and the influence of the topside connection. Moreover, analyzing the impact of the significant height and peak period, and based on the DNV rules, obtaining the limiting sea states for operating the riser system.

8.1. Quasi-static analysis

Based on the Figure6-1 and Figure7-1, which is the effective tension of the riser after the quasi-static analysis, it can be found that there is no difference between the results of two topside connection cases. So it can be inferred that the topside connection of the riser has no effect on the static analysis.

8.2. Dynamic analysis

8.2.1. Vertical displacement

From Table6-1 and 7-1, the results of the vertical displacement of end of the riser under two topside connection are very similar. It can be found that the topside connection do not influence the vertical displacement of the riser. Taking the case of pinned topside connection as an example, the impact of the wave parameters can be seen in Figure8-1.

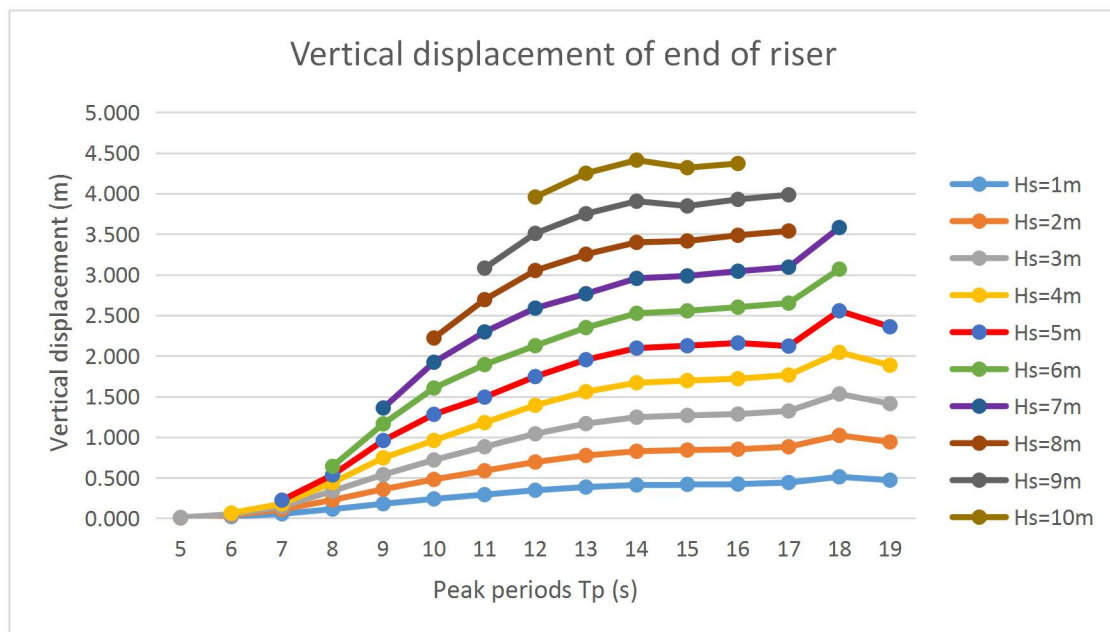


Figure 8-1. The vertical displacement of end of the riser with pinned topside connection.

From the Figure8-1, it can be found that the vertical displacement increases with the increasing of wave height. Moreover, as the wave period becomes larger, the vertical displacement increases until it stabilizes. This is according to the RAO gives for heave motion. The limiting sea states of operating the riser will be described in Section 8.2.5.

8.2.2. Axial force

As for the vertical displacement at the pump, the two kinds of topside connection cases have similar results with respect to axial tension at the top of riser. Therefore, there is no influence on the axial tension of the riser by the different topside connection. Also taking the case of pinned topside connection as an example, the impact of the wave parameters can be seen in Figure8-2.

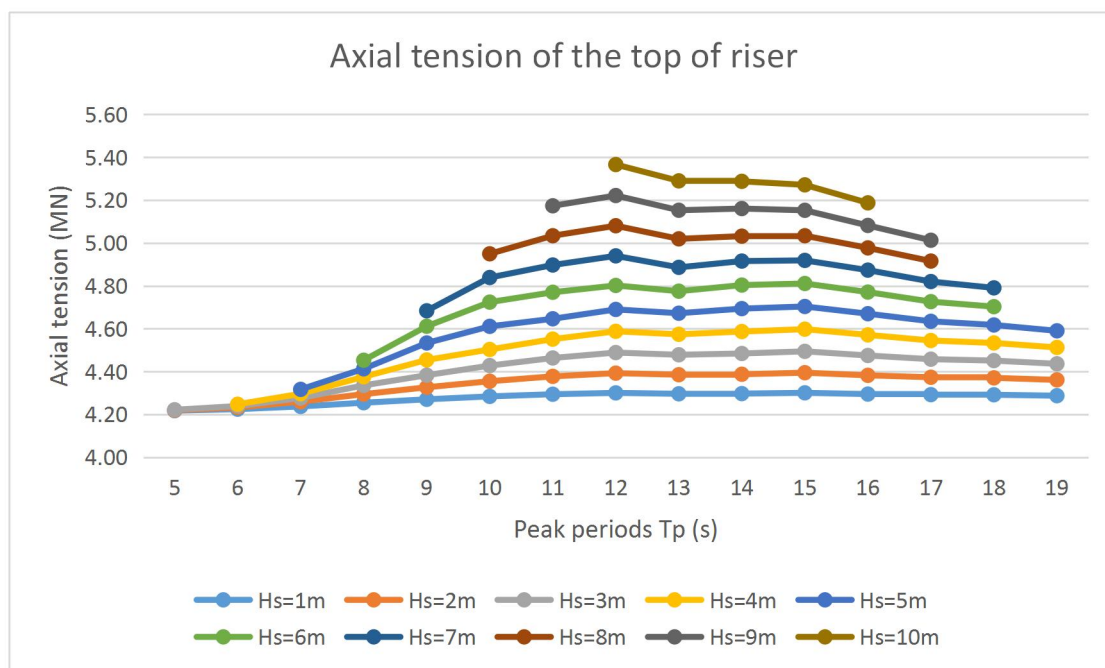


Figure 8-2. The axial tension of top of the riser with pinned topside connection.

From the Figure8-2, it can be seen that the axial tension of the top of riser increases with increasing wave height. However, at first, the axial tension becomes larger as the wave period becomes larger, when the wave period reaches a certain value, the axial tension decreases in fluctuation as the period becomes larger. This is according to the combined action of the riser dynamics and the RAOs applied for this case.

8.2.3. Bending moment

The bending moment distribution of the riser for the two kinds of topside connection cases will be different as the bending moment of riser with fixed topside connection is much larger than it with pinned topside connection. The influence of the wave

parameters on the bending moment of riser with two kinds of topside connection is shown in Figure 8-3 and 8-4.

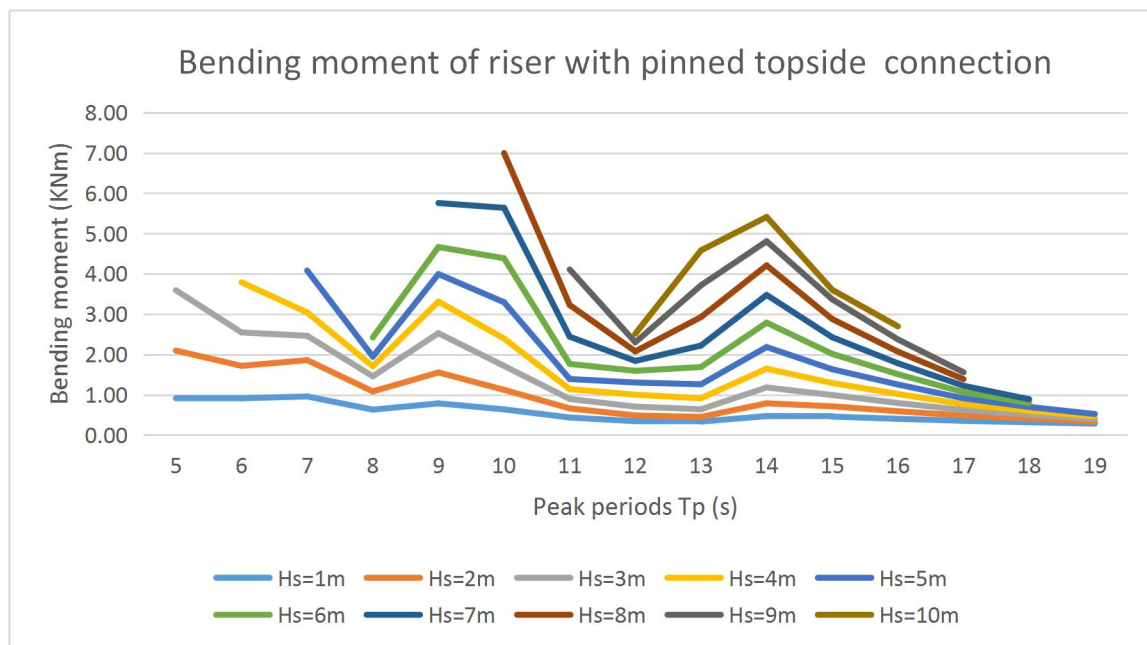


Figure 8-3. The maximum bending moment of riser with pinned topside connection.

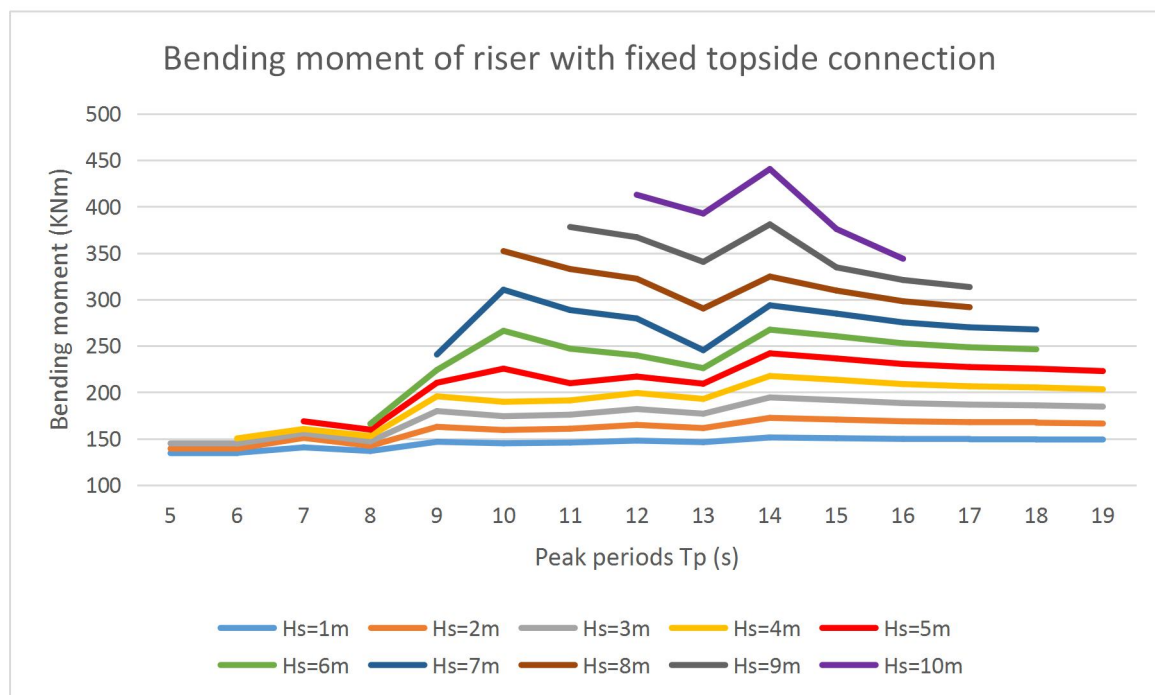


Figure 8-4. The maximum bending moment of riser with fixed topside connection.

The bending moment of riser with the two kinds of topside connection is increasing as a result of growing wave height. However, the maximum bending moment does not show a regular change with the increase of the wave period, which is related to the combined action of vessel motion, riser dynamics and local wave loads at the top.

8.2.4. Riser stress

Due to the great difference in bending moments for the two topside connection cases, the maximum stress of riser with fixed topside connection is much larger than it with pinned topside connection. The impact of the wave parameters on the stress of riser with two kinds of topside connection can be shown in Figure 8-5 and 8-6.

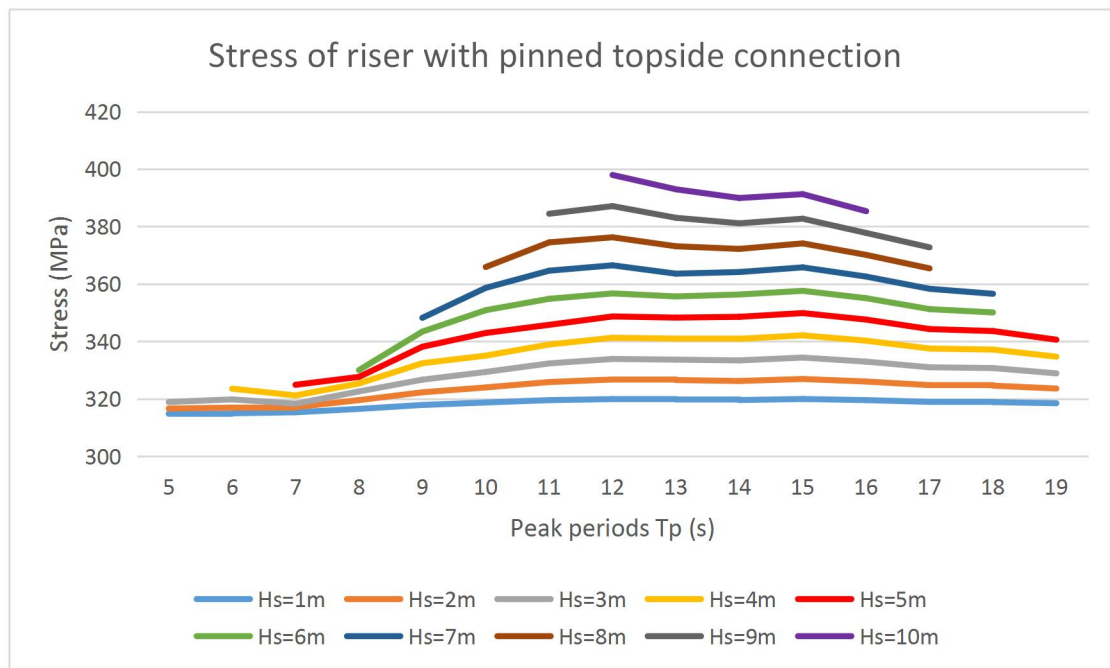


Figure 8-5. The maximum stress of riser with pinned topside connection.

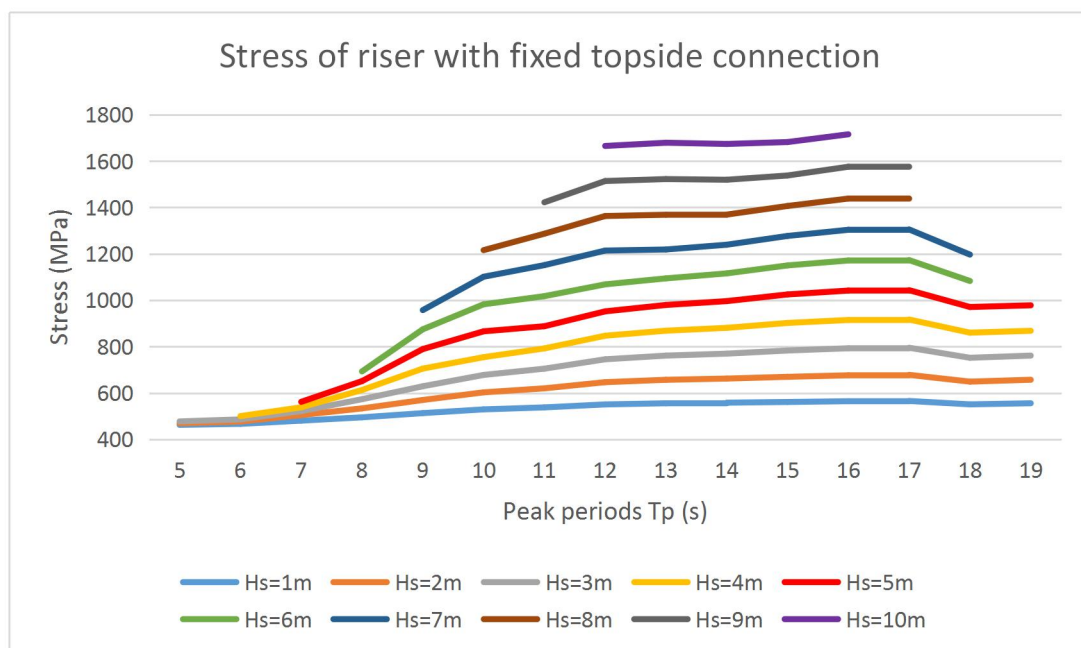


Figure 8-6. The maximum stress of riser with fixed topside connection.

The riser stress is increasing with growing wave height in both cases. For the fixed topside connection case, the stress is increasing as the wave period increased. However, for the pinned topside connection case, it is first rising then declining. This is in accordance with the previous observation that the pinned case dynamics is more governed by tension dynamics. Whereas for the fixed case, the maximum riser stress will be governed by the combined effects of quasi-static tension and pitch motion.

8.3. Limiting sea states

Based on the results of dynamic analysis, the limiting sea states for operating the riser system can be defined.

The sea states that produce the condition of the vertical displacement of the end of riser is larger than the 1/1000 of the riser length, which is 2.97m, can be considered as limiting sea states. By this criteria, in the selected wave scatter diagram, the limiting sea states is marked by yellow colour in the Table8-1.

Table 8-1. The limiting sea states for operating the riser system

<div style="display: inline-block; transform: rotate(-45deg);">Tp</div> <div style="display: inline-block; transform: rotate(45deg);">Hs</div>	11	12	13	14	15	16	17	18	19
6	1,893	2,126	2,349	2,525	2,555	2,601	2,650	3,069	X
7	2,296	2,589	2,766	2,956	2,986	3,043	3,094	3,582	X
8	2,694	3,052	3,253	3,399	3,417	3,486	3,539	X	X
9	3,082	3,510	3,752	3,906	3,847	3,928	3,985	X	X
10	X	3,957	4,250	4,412	4,319	4,370	X	X	X

Moreover, related to the DNV rules in the Section 3.1.3, riser system subjected to the bending moment and effective tension shall be designed to satisfy Eq.(3-1). Including the related parameters in Table5-2, the (plastic) bending moment resistance and the plastic axial force resistance is obtained by Eq.(3-2) and Eq.(3-3), which is shown as follows:

$$\begin{aligned}
 M_k &= 386 * 1.2 * (0.3 - 0.015)^2 * 0.015 = 0.6 \text{ MNm} \\
 T_k &= 386 * 1.2 * \pi * (0.3 - 0.015) * 0.015 = 6.22 \text{ MN}
 \end{aligned}
 \tag{8-1}$$

Then the data of total bending moment and axial tension will be imported in the formula to check if the riser system can be operated in the selected sea states.

Table 8-2. Riser stress checking by DNV rules in the pinned topside connection.

Tp Hs	5	6	7	8	9	10	11	12	13	14	15	16	17	18	19
1	0.605	0.607	0.610	0.615	0.620	0.623	0.626	0.627	0.626	0.627	0.628	0.626	0.625	0.625	0.623
2	0.608	0.611	0.619	0.627	0.638	0.645	0.651	0.655	0.653	0.654	0.656	0.652	0.649	0.648	0.645
3	0.612	0.614	0.625	0.640	0.656	0.668	0.677	0.684	0.681	0.684	0.687	0.680	0.675	0.672	0.668
4		0.619	0.632	0.652	0.679	0.692	0.704	0.715	0.711	0.716	0.719	0.710	0.702	0.698	0.691
5			0.640	0.664	0.705	0.728	0.734	0.748	0.742	0.751	0.753	0.742	0.730	0.724	0.715
6				0.677	0.731	0.766	0.775	0.785	0.776	0.788	0.789	0.774	0.759	0.751	
7					0.756	0.806	0.818	0.831	0.814	0.826	0.825	0.809	0.790	0.780	
8						0.845	0.866	0.879	0.860	0.867	0.865	0.844	0.822		
9							0.916	0.929	0.908	0.913	0.907	0.880	0.855		
10								0.981	0.958	0.959	0.949	0.918			

Table 8-3. Riser stress checking by DNV rules in the fixed topside connection.

Tp Hs	5	6	7	8	9	10	11	12	13	14	15	16	17	18	19
1	0.896	0.899	0.915	0.912	0.938	0.939	0.943	0.950	0.945	0.956	0.955	0.952	0.950	0.950	0.947
2	0.907	0.911	0.944	0.936	0.990	0.991	1.000	1.014	1.004	1.029	1.027	1.019	1.015	1.012	1.008
3	0.920	0.925	0.960	0.958	1.044	1.045	1.059	1.080	1.066	1.106	1.103	1.090	1.081	1.077	1.070
4		0.940	0.976	0.982	1.100	1.102	1.120	1.148	1.130	1.188	1.183	1.164	1.151	1.145	1.134
5			1.000	1.009	1.156	1.213	1.190	1.219	1.197	1.275	1.266	1.242	1.224	1.215	1.201
6				1.034	1.210	1.338	1.310	1.305	1.266	1.366	1.353	1.323	1.300	1.288	
7					1.269	1.472	1.443	1.438	1.345	1.460	1.442	1.406	1.377	1.362	
8						1.599	1.586	1.579	1.488	1.567	1.535	1.491	1.456		
9							1.733	1.726	1.644	1.735	1.631	1.576	1.536		
10								1.878	1.806	1.910	1.763	1.663			

Based on the Table8-2 and 8-3, it can be seen that in the pinned topside connection case, the results of all sea states satisfy the DNV rules. But in the fixed topside connection case, the results of most of sea states do not satisfy the DNV rules. This means that riser load out can only be done for the sea states in the range of Hs is 1m. Therefore, for the pinned topside connection case, the limiting sea states are selected by the vertical displacement of the end of riser, which is shown in Table8-1. What is more, for the fixed topside connection case, the limiting sea states are selected by the DNV stress rules, which is shown in Table8-3.

8.4. Fatigue analysis

The results of the riser fatigue life in different conditions are shown in Table8-4.

Table 8-4. The riser fatigue life in different conditions.

	Resultant stress	Axial tension stress	Bending moment stress
Pinned topside connection	3 weeks	One month	113 years
fixed topside connection	15 minutes	One month	15 minutes

From the Table8-4, it can be found that in the pinned topside connection case, the axial tension has a big impact on the fatigue life of the riser. However, in the fixed topside connection case, the bending moment has a big impact on the fatigue life of the riser.

9. Conclusion and further work

9.1. Conclusion

Consequently, the topside connection of the riser has a big impact on the bending moment of the riser. The bending moment of the riser with fixed topside connection is much larger than it with pinned topside connection. And therefore affect the stress and fatigue life of the riser. Moreover, in the dynamic analysis, all the response of riser is increasing as the growing of the wave significant height. However, there is a complex relationship between the wave peak period and the riser response. When the wave peak period is increasing, the changing of the riser response is the result of a combination of vessel motion, local wave loads and riser dynamics. Furthermore, the limiting sea states of the riser with pinned topside connection is when the wave significant height is larger than 7m. And to the fixed topside connection is when the wave significant height is larger than 2m. In addition, in this case, the fatigue life of the riser is too short whatever the topside connection is. Although the riser is installed segmentally and the time of installation of the riser with fixed topside connection is short, the fatigue life of the riser system is still relatively short. Not to mention during the normal operation of the riser with pinned topside connection, the fatigue life is still only around one month. In conclusion, it is difficult to apply a steel riser under these conditions, even if the vortex induced vibration is not considered in this study. The one method of increasing the fatigue life of riser is to decrease the axial tension by increasing the buoyancy layer outside the riser wall.

9.2. Further work

For improving the riser response and the fatigue life, these are some further work can be implemented. Firstly, optimizing the distribution of the steel riser thickness and its buoyancy. Then the inner mineral density can be lower than 2000 kg/m^3 , which can be around 1300 kg/m^3 . Moreover, the selected sea states can only be considered the summer condition, it will give better sea states. In addition to the improvement work, this study needed to consider more detailed requirements. For the riser modelling, because the riser is too long, taking into account the actual installation and operation process of the riser, it is needed to establish some booster stations along the riser. Then, there are more riser configurations needed to be applied in the fixed topside connection case. Moreover, during the fatigue analysis procedure, the effect of vortex induced vibration and the directionality should be considered. On account of the semi-submersible platform represents a lower bound vessel motion, FPSO or other mining support vessels can be as an alternate. Last but not the least, the flexible pipe technology can be applied in this study field.

Reference

- [1] Deep water mining in Norway. October 21, 2013. Retrieved from: <https://www.sciencedaily.com/releases/2013/10/131021094726.htm>
- [2] B. G. Burke. (1974). An Analysis of Marine Risers For Deep Water. DOI : <https://doi.org/10.4043/1771-MS>
- [3] Chen J .etc. (2012). Dynamic response and fatigue damage analysis for drilling riser. *Proceedings of 2012 International Conference on Mechanical Engineering and Material Science (MEMS 2012)*, 704-707.
- [4] Mukundan H. etc. (2009). Monitoring VIV fatigue damage on marine risers. *Journal of Fluids and Structures*. Volume 25, Issue 4, May 2009, Pages 617-628
- [5] James R. etc. (2012). Deep-ocean mineral deposits as a source of critical metals for high- and green-technology applications: Comparison with land-based resources. *ORE GEOLOGY REVIEWS*. DOI: 10.1016/j.oregeorev.2012.12.001
- [6] R.E.Boschen. etc. (2013). Mining of deep-sea seafloor massive sulfides: A review of the deposits, their benthic communities, impacts from mining, regulatory frameworks and management strategies. DOI: <https://doi.org/10.1016/j.ocecoaman.2013.07.005>
- [7] Porter H. etc. (2009). Deep-sea mining of seafloor massive sulfides. DOI: <https://doi.org/10.1016/j.marpol.2009.12.001>
- [8] Marine Assets Corporation's (MAC) Seabed Mining Vessel. Retrieved from: <http://www.ship-technology.com/projects/marine-assets-corporations-mac-seabed-mining-vessel/>
- [9] OFFSHORE STANDARD. DNV-OS-F201 (OCTOBER 2010). DYNAMIC RISERS
- [10] RECOMMENDED PRACTICE. DNV-RP-F204 (OCTOBER 2010). RISER FATIGUE
- [11] RECOMMENDED PRACTICE. DNV-RP-C203 (OCTOBER 2011). Fatigue Design of Offshore Steel Structures
- [12] In FEA, what is linear and nonlinear analysis. Retrieved from: <https://www.femto.eu/stories/linear-non-linear-analysis-explained/>
- [13] SIMA is developed by Norwegian Marine Technology (MARINTEK)
- [14] Malvern, L.E. (1969). Introduction to the Mechanics of a Continuous Medium. Prentice Hall, Englewood Cliffs, New Jersey.
- [15] Mollestad, E. (1983). Techniques for Static and Dynamic Solution of Non-linear Finite Element Problems. Report No. 83-1, Div. of Structural Mechanics, Norwegian Institute of Technology, Trondheim.
- [16] Torgeir Moan(2013). Finite element modelling and analysis of marine structures. Department of Marine Technology, Norwegian University of Science and Technology
- [17] Liping S. etc. (2011). Global Analysis of a Flexible Riser. *Marine. Sci. Appl.* 2011. 10: 478-484
- [18] Forristall, G.Z. (2000). Wave Crest Distributions: Observations and Second-Order Theory. *Journal of Physical Oceanography* 30 1931.
- [19] The JONSWAP spectra in the wave-frequency domain. Retrieved from:

http://www.codecogs.com/library/engineering/fluid_mechanics/waves/spectra/jo_nswap.php

- [20] Remseth, S.N. (1978). Nonlinear Static and Dynamic Analysis of Space Structures. Dr.ing. Thesis, Report No. 78-2, Division of Structural Mechanics, The Norwegian Institute of Technology, Trondheim.
- [21] O.M.Faltinsen. Sea loads on ships and offshore structures. Department of Marine Technology, Norwegian Institute of Technology, Trondheim.
- [22] Rommel B.B. etc. FATIGUE ANALYSIS OF RISERS. Proceedings of IPC' 02 4th International Pipeline Conference September 29-October 3, 2002, Calgary, Alberta, Canada.
- [23] John Wægter. Stress range histories and Rain Flow counting. June 2009
- [24] RECOMMENDED PRACTICE. DNV-RP-C205 (APRIL 2007). Environmental conditions and environmental loads.